Journal Pre-proof

A Triassic to Jurassic arc in north Borneo: Geochronology, geochemistry, and genesis of the Segama Valley Felsic Intrusions and the Sabah ophiolite

A. Burton-Johnson, C.G. Macpherson, I.L. Millar, M.J. Whitehouse, C.J. Ottley, G.M. Nowell

PII: S1342-937X(20)30120-9

DOI: https://doi.org/10.1016/j.gr.2020.03.006

Reference: GR 2333

To appear in: *Gondwana Research*

Received date: 8 November 2019

Revised date: 16 March 2020

Accepted date: 20 March 2020

Please cite this article as: A. Burton-Johnson, C.G. Macpherson, I.L. Millar, et al., A Triassic to Jurassic arc in north Borneo: Geochronology, geochemistry, and genesis of the Segama Valley Felsic Intrusions and the Sabah ophiolite, *Gondwana Research* (2020), https://doi.org/10.1016/j.gr.2020.03.006

This is a PDF file of an article that has undergone enhancements after acceptance, such as the addition of a cover page and metadata, and formatting for readability, but it is not yet the definitive version of record. This version will undergo additional copyediting, typesetting and review before it is published in its final form, but we are providing this version to give early visibility of the article. Please note that, during the production process, errors may be discovered which could affect the content, and all legal disclaimers that apply to the journal pertain.

© 2020 Published by Elsevier.

Journal Pre-proof

A Triassic to Jurassic arc in north Borneo: Geochronology, geochemistry, and genesis of the Segama Valley Felsic Intrusions and the Sabah ophiolite

Burton-Johnson, A[a*], Macpherson, C.G.[b], Millar, I.L.[c], Whitehouse, M.J.[d], Ottley, C.J.[b], Nowell, G.M.[b]

[a]British Antarctic Survey, High Cross, Madingley Road, Cambridge, CB3 0ET, UK

[b]Department of Earth Sciences, University of Durham, Durham, DH1 3LE, UK

[c]British Geological Survey, Keyworth, Nottingham NG12 5GG, UK

[d]Swedish Museum of Natural History, Box 50007, SE-104 05 Stockholm, Sweden

*Author for correspondence

e-mail: alerto@bas.ac.uk

Keywords

SE Asia, Borneo, Tectonics, ophiolite, Paleo-Pacific

Highlights

1) The Sundaland Paleo-Pacific arc continued into north Borneo from the Triassic
2) There is no evidence for continental basement in the Segama Valley
3) The oldest basalts of the Sabah ophiolite are least Triassic in age

Journal Pre-proof

Journal Pre-proof

Abstract

New field, geochemical, and geochronological data from the Segama Valley Felsic Intrusions (SVFI) of Sabah, north Borneo, shows them to be arc-derived tonalites; not windows or partial melts of a crystalline basement beneath Sabah. U-Pb zircon ages date emplacement in the Triassic and Jurassic: 241.1±2.0 Ma, 250.7±1.9 Ma, 178.7±2.4 Ma, and 178.6±1.3 Ma; contemporaneous with peaks in magmatism and detrital zircons in Sarawak and west Kalimantan (west Borneo). Isotopic data for Sr, Nd, and Pb from whole rocks, and for Hf and O from zircon all show mantle and/or MORB affinities indicating a mantle-derived origin. Enrichment of fluid mobile trace elements and trace element ratios indicate that the most likely setting for this is in a continuation of the Sundaland continental arc. There is no evidence in the field, geochemical, or zircon U-Pb data for continental basement in the Segama Valley region.

The intrusive nature of the Segama Valley tonalites constrains the emplacement age of their supra-subduction zone host rocks to at least the Triassic. This new data expands the Triassic and Jurassic extent of Borneo and the Sundaland arc, and challenges models of Borneo's development predominantly through allochthonous terrane accretion in the Cretaceous. Instead, we propose a model of protracted autochthonous growth through supra-subduction zone crustal extension and associated magmatism.

Journal Pre-proof

1. Introduction

The nature of the basement beneath the Malaysian state of Sabah, North Borneo, remains debated (e.g. Graves et al., 2000; Hutchison, 2005; Leong, 2017, 1998, 1974; Milsom et al., 2001). The exposed geology is predominantly of Cenozoic marine sediments underlain by an ophiolite sequence exposed near the Segama Valley, Darvel Bay, Telupid, Mt Kinabalu, and Kudat (Fig. 1). However, an extensive "crystalline basement" of unexposed granitic continental crust has been proposed on the basis of three main lines of evidence (Hutchison, 2005; Kirk, 1968; Leong, 1974; Reinhard and Wenk, 1951): First, gravity data shows an extensive low gravity anomaly over much of Sabah that has been interpreted to result from low density continental crust beneath the region (Holt, 1998; Milsom et al., 2001). Second, Plio-Pleistocene volcanics of the Semporna peninsula in E Sabah (Fig. 1) and the Usun Apau plateau of Sarawak, NW Borneo (Fig. 2) have anomalously low Nd isotopic values that have been attributed to assimilation of Proterozoic continental crust by mantle melts (Cullen et al., 2013; Macpherson et al., 2010). Third, calc-alkaline granitic bodies have been mapped within the ophiolite of the Segama Valley (Fig, 1; Kirk, 1968; Leong, 1974), postulated to be partial melts or windows of an underlying continental basement (Hutchison, 2005).

The gravitational evidence and geochemistry of Plio-Pleistocene volcanic rocks rely on interpretation of data relating to unexposed crust, and thus are not corroborated by direct observation. However, the granitic bodies of the Segama Valley can be mapped and sampled for geochemical analysis. If they are indeed windows of continental basement, then we would expect them to pre-date the ophiolite (i.e. not display intrusive contacts), and display evidence for a continental origin and/or crustal assimilation in their isotopic compositions and U-Pb zircon ages.

This work presents the first new geochronological and geochemical study of the Segama Valley intrusive bodies since Kirk (1968) and Leong (1974). In addition to re-evaluating their field relations, we have conducted major and trace element analysis; measured Sr, Nd, Pb and O isotope ratios; and performed U-Pb zircon

geochronology. We use the results to discuss the implications for genesis of the Sabah ophiolite and the nature of the north Borneo basement.

2. Regional Geological History

During the Mesozoic, a continental arc existed across Sundaland and East Asia. This extended from the Yanshanian province of SE China, across the continental crust of the South China Sea continental shelf, along Vietnam and Peninsular Malaysia, to the Schwaner Mountains of Kalimantan in SW Borneo (Metcalfe, 2011). The arc produced a belt of granites and lesser volcanics across SE Asia, hundreds of kilometres wide (Fig. 2).

The Mesozoic also saw emplacement of the ophiolitic basement in north and east Borneo, which is preserved as a belt stretching from central Java, across the Meratus Mountains and Sabah in Borneo, and into Palawan and the Philippines (Fig. 1 and 2). Although some studies have proposed a mid-ocean ridge setting for formation of the Sabah ophiolite (Graves et al., 2000), LILE and HFSE data has been used to infer formation in a supra-subduction zone setting (Omang and Barber, 1996). The age of the Sabah ophiolite is unclear, with mafic amphibolites giving K-Ar radiometric ages ranging from 127-87 Ma (Kirk, 1968; Leong, 1974; Omang, 1993; Swauger et al., 1995), gabbros giving 179-33.4 Ma K-Ar ages (Graves et al., 2000; Omang, 1993; Rangin et al., 1990), and the overlying cherts giving 127-135 Ma biostratigraphic ages (Jasin, 1992).

Granitic bodies were mapped within the ophiolite and interpreted as windows of an underlying basement of continental crust (the “crystalline basement”). These felsic rocks yielded K-Ar ages of 210-120 Ma (Kirk, 1968; Leong, 1998, 1974), although the Triassic and Early Jurassic ages have been questioned and excluded from later studies for being older than the Cretaceous ages obtained for the ophiolitic units, viewing them all as part of the same ophiolite suite (Hutchison, 2005, 1988; Omang and Barber, 1996).

Borneo became the location of extensive marine sedimentation through the Cenozoic, during which most of its extensive cover of marine mudstones and turbidites were deposited (Fig. 1; Collenette, 1965; van Hattum et al., 2006). These deposits are dominated by Eocene to Miocene deep marine turbidites,

forming the large, SW-NE trending Crocker Basin (Fig. 1). Folding and faulting of the basement and cover rocks occurred in the Eocene and Oligocene, driven by subduction of the proto-South China Sea or other collisional tectonic processes (Hall, 1996; Hall and Wilson, 2000; Hutchison, 2000; Rangin and Silver, 1990; Taylor and Hayes, 1983; Tongkul, 1994, 1991). Further turbidite sedimentation continued into the Miocene, when carbonates and shallow marine to fluvial deltaic deposits formed in a shallower marine setting (Balaguru, 2001). The Early Miocene collision of northern Borneo and the South China continental margin drove the Sabah orogeny (Hall and Wilson, 2000; Hutchison, 2000, 1996), producing significant topography in the region and the emergence of much of Sabah and the present central highlands of northern Borneo (Hutchison, 2000).

3. Field data and petrography

3.1. Ophiolite in the Segama Valley

Outcrops in the Segama Valley of Eastern Sabah form part of the Sabah ophiolite. Kirk (1968) and Leong (1974) differentiated the Mesozoic basement of Sabah into a sequence of (1) dolerites, gabbros, and variably serpentinised peridotites; (2) metamorphic amphibolites, schists and gneisses; (3) the Chert-Spilite Formation of marine sediments and basaltic submarine volcanism; and (4) felsic intrusions (termed the "crystalline basement" in those studies). However, subsequent understanding of ophiolite stratigraphy indicates that ophiolites represent oceanic crust emplaced in a submarine spreading centre or marginal basin, (Pearce, 2003). On this basis, all the Mesozoic basement units, except for the felsic intrusions, can be interpreted as constituent parts of an ophiolite, representing variably metamorphosed mafic intrusive crust (1 and 2), associated extrusive magmatism (3, the spilites), and overlying marine sedimentation (3, the cherts). As noted by Hutchison (2005), ribbon cherts represent the first sediments to be deposited on newly emplaced seafloor, explaining the abundance of this lithology in the Chert-Spilite Formation

3.2. The Segama Valley Felsic Intrusions (SVFI)

Intrusive bodies of tonalite, granodiorite and granite up to 5km long were recorded by Leong (1974) as outcrops within the Segama Valley ophiolite, and are referred to here as the Segama Valley Felsic Intrusions (SVFI). These outcrops were mapped in Dismal Gorge and the Barrier Falls on Sungai (S.; "river" in Malay) Segama; S. Purut; Danum Gorge; S. Telewas; and the S. Litog Klikog Kiri and S. Babayas tributaries of S. Segama (Fig. 3). We visited the S. Purut, S. Danum, Barrier Falls and the S. Litog Klikog Kiri/S. Babayas intrusions, although the meander mapped as the Barrier Falls intrusion Leong (1974) was found to be composed of mudstone and chloritised mafic rocks. To determine compositions, mineral abundances were calculated from point counting thin sections stained for plagioclase and K-feldspar. QAP modal mineral classifications are shown in Fig. 4.

3.2.1. The S. Purut Intrusion

S. Purut is a tributary of the Upper S. Segama. The felsic intrusion is a medium-grained tonalite composed of 11% quartz, 22% plagioclase, and 16% hornblende (A245). Chlorite and sericite form 13% and 38%, respectively, which if derived solely from the hornblende and plagioclase puts their respective percentages at 29% and 60%. The body has an intrusive contact with basaltic country rocks, with xenoliths of the basaltic country rock within the granite (Fig. 5a) and abundant small wispy chloritised xenoliths of the country rock within the tonalite near the contact. The country rock is rich in amygdales, chlorite, zeolite and quartz (indicating shallow water crystallisation), which have altered to a highly chloritised hornfels along the contact. Kirk (1968) assigned this unit to the spilite of the "Chert-Spilite Formation".

3.2.2. S. Danum Intrusion

The S. Danum intrusion forms the walls of the narrow, 800m long Danum Gorge. This is another medium-grained tonalite composed of 25% quartz, 56% plagioclase, 5% alkali feldspar, and 14% variably chloritised hornblende (A249). The body intrudes microcrystalline quartzite country rock, and a thick band of chloritised country rock exists on its margin (Fig. 5b and 5c). Adjacent to this

band of alteration, the quartzite is preferentially hardened by recrystallisation (a baked margin). Wispy xenoliths of the chloritised country rock occur within the tonalite. Further downstream, fine-grained, 10-40m wide, phaneritic dacite dykes and intrusions intrude the quartzite. However, these dykes are not exposed in contact with the tonalite, and so the relationship of the two magmatic events is unknown.

3.2.3. The Litog Klikog Kiri (S. LKK.) Intrusion.

The S. Litog Klikog Kiri (S. LKK.) intrusion lies between S. LKK. and S. Babayas; two small tributaries of the Middle S. Segama. The intrusion is a medium-grained tonalite of 28% quartz, 61% plagioclase, 3% alkali feldspar, and 8% chloritised hornblende (A261). Upstream outcrops are richer in biotite being composed of 22% quartz, 44% plagioclase, 3% alkali feldspar, 17% hornblende, 7% biotite, and 7% chlorite (A265). These distinct mineralogies may represent construction of the intrusion from multiple pulses of magma. The S. LKK. stream follows the intrusive contact between the felsic intrusion and the intruded hornfelsed country rock, which is a highly chloritised basalt composed of plagioclase-rich groundmass, variably chloritised clinopyroxene phenocrysts, and calcite amygdales. In one outcrop, the protolith has been entirely altered to biotite.

The S. Babayas stream follows a biotite-rich mafic hornfels along the intrusion's eastern contact. However, although tonalitic dykes are observed, the main body is not exposed in S. Babayas. Calc-silicate rocks are exposed in the stream, and are in faulted contact with the mafic hornfels at both ends of their extent.

4. Analytical methodology

4.1. Major and trace elements

Samples of the Segama Valley Felsic Intrusions (SVFI) and country rock were analysed for major element composition by XRF at Edinburgh University, and by ICP-MS and PIMMS (Plasma Ionisation Multi-collector Mass Spectrometry) at Durham University to obtain trace element and radiogenic isotope data.

Samples were crushed and milled to a fine powder using a fly press and agate ball mills. For XRF analysis the samples were dried at 1100°C to calculate Loss On Ignition (LOI) before being mixed with $LiBO_2$ flux and fused into glass discs for analysis (Gill, 1997). Trace element analysis followed the procedure of Ottley et al. (2003). Samples were dissolved using HF and HNO_3, and analysed on a ThermoScientific X-Series 2 ICP-MS. Elements affected by incomplete zircon dissolution were analysed by the same procedure after the sample was first fused with a $LiBO_2$ flux. These elements are: Ta, Cs, Zr, Hf, Th, U, Nd, Y, and the REE (excluding La, for which the $LiBO_2$ flux affects analytical accuracy). Accuracy and reproducibility were determined by repeat analysis of the standards, AGV-1, BHVO-1, and W2, as well as two samples from Mt Kinabalu (Burton-Johnson et al., 2019). Acid blanks and the $LiBO_2$ flux were also analysed. This QC data is presented in the supplementary material.

4.2. Whole rock radiogenic isotope analysis

Sample preparation for Sr and Nd isotopic analysis followed the column chemistry procedures of Charlier et al. (2006). Whole rock powders were dissolved in HF and HNO_3 SpA acid and separated by column chemistry using Sr-spec resin and Hf-Nd cation resin (AG50 X-8). A Pb fraction was collected in 100µl 8N HCl from the Sr columns following collection of the Nd and Sr fractions and waste elution using 200µl 2.5N HCl. The Pb fraction was then dried down, dissolved in 500µl 3% HNO_3, and spiked with ^{206}Tl to correct for mass bias (Hirata, 1996). PIMMS analytical procedures following Nowell et al. (2003). For $^{87}Sr/^{86}Sr$ and $^{143}Nd/^{144}Nd$, measured values for the NBS987 and J&M standards (±2SD error) during the same run as the samples were 0.710267 ±23 (n=35) and 0.511109 ±10 (n=44) respectively. Data are corrected to the respective NBS987 and J&M standard values of 0.71024 (Thirlwall, 1991) and 0.511110 (Royse et al., 1998). For Pb, measured values for the NBS981 standards ±2SD for $^{206}Pb/^{204}Pb$, $^{207}Pb/^{204}Pb$, $^{208}Pb/^{204}Pb$, $^{207}Pb/^{206}Pb$ and $^{208}Pb/^{206}Pb$ (n=12) are 16.9405 ±9, 15.4983 ±9, 36.7181 ±21, 0.9149 ±1 and 2.1675 ±5, respectively. Data are corrected to values of NBS981 of 16.9405, 15.4980, 36.7174, 0.91485 and 2.1674, respectively (Galer, 1997).

4.3. Zircon U-Pb geochronology

For U-Pb analysis, zircon crystals were separated from <500 μm sieved fractions of powdered samples by panning, and then handpicking before mounting in epoxy and polishing. Their internal structure was imaged by cathodoluminescence (CL) at the University of Edinburgh, UK. U-Pb isotopic analysis was performed on a Cameca ims-1270 ion microprobe at the University of Edinburgh following the procedures of Kelly et al. (2008). Results were calibrated against zircon Geostandard 91500, which has a $^{206}Pb/^{238}U$ ratio of 0.17918±8, a $^{206}Pb/^{238}U$ age of 1062.5±0.4 Ma, and U and Pb concentrations of 81.2 and 14.8 ppm, respectively (Wiedenbeck et al., 1995). $^{206}Pb/^{238}U$ concordia ages were calculated using Isoplot v3.7 (Ludwig, 2003). Uncertainty in the calculated pluton ages are presented as 95% confidence limits.

4.4. Zircon Hf isotopic analysis

Isotope analyses were carried out at NIGL using a Thermo Scientific Neptune Plus MC-ICP-MS coupled to a New Wave Research UP193UC Excimer laser ablation system. Helium was used as the carrier gas through the ablation cell with Ar make-up gas being connected via a T-piece and sourced from a Cetac Aridus II desolvating nebulizer. 0.006 l/min of nitrogen was introduced via the nebulizer in addition to Ar in order to minimise oxide formation. Lutetium (^{175}Lu), Ytterbium (^{172}Yb, ^{173}Yb), and Hafnium (^{176}Hf, ^{178}Hf, ^{179}Hf and ^{180}Hf) isotopes were measured simultaneously during static 30 second ablation analyses.

Hf reference solution, JMC475 was analysed during the analytical session and $^{176}Hf/^{177}Hf$ ratios of unknown samples are reported relative to a value of 0.282160 for this standard. Correction for ^{176}Yb on the ^{176}Hf peak was made using reverse-mass-bias correction of the $^{176}Yb/^{173}Yb$ ratio. This $^{176}Yb/^{173}Yb$ ratio was empirically derived using Hf mass bias corrected Yb-doped JMC475 solutions (Nowell and Parrish, 2001). ^{176}Lu interference on the ^{176}Hf peak was corrected by using the measured ^{175}Lu and assuming $^{176}Lu/^{175}Lu = 0.02653$. Hf-isotope data was processed using the Iolite data reduction package (Paton et al., 2011).

Journal Pre-proof

Three zircon reference materials (91500, Mud Tank, Plesovice) were analysed throughout the analytical session. The 91500 zircon reference material was used as the primary standard in Iolite, and was used to normalise the $^{176}Lu/^{177}Hf$ ratio assuming a value of 0.000311 (Woodhead and Hergt, 2005).

Analytical uncertainties for unknowns were propagated by quadratic addition to include the standard error of the mean of the analysis, and the reproducibility of the 91500 reference material. εHf values were calculated using a ^{176}Lu decay constant of 1.867 x 10-11y^{-1} (Söderlund et al., 2004), the present-day chondritic $^{176}Lu/^{177}Hf$ value of 0.0336, and a $^{176}Hf/^{177}Hf$ ratio of 0.282785 (Bouvier et al., 2008).

4.5. Zircon $\delta^{18}O$ analysis

Oxygen isotope analyses were performed on the zircon crystals analysed for U-Pb using a CAMECA IMS 1280 large geometry SIMS at the NordSIMS facility in Stockholm, Sweden, using the methods of Whitehouse and Nemchin (2009). A critically focused Cs^+ primary beam with 20 keV impact sputtered the sample, and a low-energy electron-flooding gun was used for charge compensation. The primary beam current was ca. 2 nA yielding a ca. 15 μm analytical spots, including a 10 μm raster to homogenize the beam. Each analysis consisted of an initial pre-sputter over a rastered 20 μm^2 area to remove the gold coating, followed by secondary beam centering in the field aperture (field of view was 30 μm with 90x magnification transmission ion optics). The ^{16}O (ca. 2 x 10^9 cps) and ^{18}O ion beams were mass filtered at a mass resolution of ca. 2500 (M/ΔM) and analysed simultaneously using two Faraday detectors with amplifiers housed in an evacuated, temperature stabilized chamber. The secondary magnet field was locked at high stability using an NMR field sensor operating in regulation mode. All pre-sputter, beam centering and data acquisition steps were automated in the run definition. Typical internal precision obtained for individual run $^{18}O/^{16}O$ ratios determined from 12 4-second integrations was ca. 0.1 ‰ (SE).

Journal Pre-proof

Fully automated sequences comprised two measurements of the reference zircon, Geostandard 91500 (Wiedenbeck et al., 2004), bracketing six measurements of unknown targets. The regularly interspersed 91500 measurements were used to correct measured isotope ratios for any drift during the analytical session and for instrumental mass fractionation (IMF), assuming a $\delta^{18}O_{V\text{-}SMOW}$ for 91500 of 9.86 ‰. External precision on $\delta^{18}O_{V\text{-}SMOW}$ was 0.16 ‰ (SD) and is propagated onto the internal precision to yield the overall uncertainty. Three analyses of the Temora-2 zircon standard yield a weighted $\delta^{18}O_{V\text{-}SMOW}$ of 8.24±0.11 ‰ (SD), which is within error of the 8.20±0.01 ‰ value reported by Black et al. (2004).

5. Results

5.1. Zircon U-Pb geochronology

Results of zircon U-Pb analyses are reported in Table 2. $^{238}U/^{206}Pb$ concordia and CL images of representative analyses are shown in Fig. 6. Two of the SVFI samples (A245, S. Purut, and A249, S. Danum) yield Middle and Early Triassic ages (241.1±2.0 Ma and 250.7±1.9 Ma). These are the oldest high-fidelity magmatic ages so far acquired in Sabah but are comparable to Triassic ages from the West Kalimantan (Hennig et al., 2017; Setiawan et al., 2013; Williams et al., 1988) and support the previously questioned and excluded 210 Ma K-Ar age of Leong (1974). One analysis of A249 yielded a distinctly younger age (236.2±3.6 Ma) and was excluded from the concordia, with recent Pb loss the probable cause.

The two samples from the mineralogically distinct units of the S.LKK. (A261 and A265) both yielded Middle Jurassic ages (178.7±2.4 Ma and 178.6±1.3 Ma). This is slightly older than previous biotite K-Ar ages for the intrusion (150±6 Ma and 160±8 Ma; Kirk, 1968). One analysis from A261 yielded an inherited age comparable to the Triassic plutons (245.3±3.2 Ma) and was excluded from the concordia.

Journal Pre-proof

5.2. Major elements and geochemical classification

Data for all whole rock geochemical analyses are reported in Table 3. The new data for the SVFI demonstrate ranges of 55.59 to 71.39 wt. % for SiO_2 and 1.30 to 2.11 wt. % for K_2O. In the K_2O classification scheme of Le Maitre et al. (1989) the SVFI lie in the fields of calc-alkaline to high-K calc-alkaline syeno-diorite, granodiorite and granite, whereas the S. Purut volcanic rock is a tholeiitic, medium-K calc-alkaline basalt (Fig. 7 and 8a). The intrusions border the metaluminous-peraluminous boundary (Fig. 7c; molar Al/(Ca+Na+K) ranges from 0.98-1.32). These compositions are generally similar to the felsic intrusions reported by Leong (1974) and Kirk (1968), which include a small number of tholeiitic and high-K calc-alkaline rocks, but are dominantly calc-alkaline diorite, syeno-diorite, granodiorite and granite (Fig. 7).

5.3. Trace elements

Primitive mantle (PM) multi-element plots and chondrite normalised REE plots for the intrusive bodies (Fig. 9) show the LILE and LREE enrichment and HFSE and HREE depletions characteristic of arc magmatism and continental crust. This results in the classification of the SVFI as volcanic arc granitoids in tectonic discrimination diagrams (Fig. 7d; Pearce et al., 1984).

There are apparent distinctions between the two Jurassic S. LKK. samples (A261 and A265) and the two Triassic samples (A245 and A249) in their Sr, Eu, and HREE compositions. In the normalised multi-element plots (Fig. 9), the older samples show weak negative Eu anomalies and weak or absent positive Sr anomalies. In contrast, the younger S. LKK. samples show absent or weakly positive Eu anomalies and positive Sr anomalies. All of the SVFI display concave-downwards chondrite-normalised REE curves, with minima at Er, however, this is most pronounced in the most evolved S. LKK. sample, A261 (Fig. 9).

The multi-element plot for the S. Purut basalt (Fig. 9) shows a similar trace element composition to the SVFI, but a lower degree of LILE enrichment (reflecting its more mafic, less fractionated composition), and less pronounced depletion of elements compatible during fractionation of mafic to intermediate melt (Eu, Ti, and P). The LILE and LREE enrichment and HFSE and HREE

depletions again indicate an arc setting, supported by geochemical tectonic discrimination (Pearce and Cann, 1973). Published mafic samples of proposed Cretaceous age from the ophiolite in Darvel Bay (Fig. 1) range from similar arc compositions to compositions of ocean floor basalt affinity (Fig. 8; Omang and Barber, 1996).

5.4. Radiogenic isotopes

Fig. 10 shows the isotopic data acquired for the intrusive rocks and the S. Purut basalt. Correcting to the mean age of the four intrusions (212 Ma), the $^{87}Sr/^{86}Sr$, $^{143}Nd/^{144}Nd$, $^{206}Pb/^{204}Pb$, $^{207}Pb/^{204}Pb$, and $^{208}Pb/^{204}Pb$ ratios of the SVFI and the S. Purut basalt all have mantle-like values with lower Sr and Pb isotope ratios and higher Nd isotopes than bulk earth. For each of these isotope ratios, the SVFI and S. Purut basalt are indistinguishable from the range of MORB values. For regional comparison, the Plio-Pleistocene basalts of the Semporna Peninsula (80 km SE of the SVFI; Fig. 1) record variable degrees of assimilation of much older (possibly Archean) continental crust (Macpherson et al., 2010). Corrected to 212 Ma, the SVFI do not follow the isotopic assimilation trend of the Semporna Peninsula magmatism, plotting at the uncontaminated end of this range (Fig. 10).

5.5. Zircon Oxygen and Hf Isotopes

Zircon Hf and oxygen isotope ratios in the SVFI are within error of the range for mantle and MORB values (Fig. 11, Table 4). Zircon $\delta^{18}O$ is slightly lower than zircon in equilibrium with the mantle but not beyond analytical error of such values (5.3±0.3‰, Valley, 2003). Likewise, the zircon Hf isotope ratios show little variation and all fall within the range of MORB values (Fig. 11).

6. Discussion

Previous studies have proposed that the felsic intrusions of the Segama Valley region are windows of an extensive continental basement beneath the ophiolite (Hutchison, 2005; Kirk, 1968; Leong, 1974; Reinhard and Wenk, 1951). However, the contacts that we observed in the field and report here indicate that these are intrusive melts that post-date formation of the ophiolite rather than exposures of an underlying basement. As such, the SVFI offer an opportunity to

date when they were emplaced, to determine the geodynamic setting at that time, and to place minimum age constraints on the formation of ophiolitic basement in Sabah.

6.1. Origin of the Segama Valley Felsic Intrusions

Combining the trace element and isotopic data allow us to evaluate the tectonic setting in which the SVFI formed. The relative HFSE depletions and LILE enrichments of the SVFI are typical of volcanic arc granitoids (Fig. 7a and 9). Consequently, this geochemical signature was acquired either through magmatic differentiation from mafic magma in an arc setting, or was inherited through partial melting of an unexposed continental basement. The latter possibility is difficult to reconcile with the isotopic signatures of the intrusions, which plot consistently within the range of MORB values rather than towards the higher Sr, Pb and $\delta^{18}O$, and lower Nd and Hf isotope ratios expected for continental crust (DePaolo and Wasserburg, 1979; Faure, 1986). Consequently, we propose that the SVFI are the differentiated felsic magmatic products of a Jurassic and Triassic arc.

To test the interpretation of SVFI as differentiated arc magmatism we undertook fractional crystallisation modelling. Most AFC models are inappropriate for this purpose as Rhyolite-MELTS and Magma Chamber Simulator thermodynamic models are not optimised for hydrous magmatic systems involving hornblende or biotite fractionation, and mass balance equations do not reflect the changing compositions of mineral phases in response to the geochemical evolution of the magma. To address these issues, Burton-Johnson et al. (2019) developed a new approach: Equilibrated Major Element Assimilation and Fractional Crystallisation modelling (EME-AFC). This model employs two-component major element partition coefficients ($K_D^{X,Y}=(X^{Min}.Y^{Liq})/(Y^{Min}.X^{Liq})$), where X and Y are elements in a single mineral phase (^{Min}) in equilibrium with a liquid (^{Liq}). This approach allows simultaneous modelling of major elements by EME-AFC, and trace elements, radiogenic isotopes, and oxygen isotopes by recognised methods (DePaolo, 1981), with an empirical relationship to determine temperature for oxygen isotope modelling. The latest version of the EME-AFC model (v01.001; https://github.com/Alex-Burton-Johnson/EME-AFC-Modelling) was applied to

model the differentiation of the most silicic Triassic and Jurassic samples (A249 and A261) from a basaltic magma. With no proven contemporaneous basaltic samples, the composition of the S. Purut basalt was used as the primary melt, for which we assumed an initial $\delta^{18}O$ value of +5.5 ‰ (Eiler, 2001; Macpherson et al., 2000; Macpherson and Mattey, 1998; Mattey et al., 1994). Trace element partition coefficients and empirical relationships of the minor elements are from Burton-Johnson et al. (2019). Given the affinity of the SVFI isotope ratios to mantle-derived basalt, no assimilation was included during the fractional crystallisation modelling.

Within these parameters, the fractionating assemblage was modified to provide the closest agreement with the SVFI compositions (Fig. 12). Disagreements probably result from differences between the S. Purut basalt and the actual primary magma, and inaccuracies in the partition coefficients and empirical relationships employed. However, both models show that the SVFI can be generated through fractional crystallisation of an arc basalt in the absence of crustal assimilation. A249 was generated through crystallisation of 76% of the original magma volume, with the bulk fractionation of 35% clinopyroxene, 11% hornblende, 53% plagioclase, and 0.4% apatite. Similarly, A261 was generated through crystallisation of 80% of the original magma volume, with the bulk fractionation of 33% clinopyroxene, 15% hornblende, 51% plagioclase, and 0.4% apatite, plus 0.8% garnet. This garnet fractionation only occurred in the final stage of the magma evolution (SiO_2> 63 wt. %), as evidenced by the Sr/Y-SiO_2 variation of the SVFI (Fig. 12a.7 and Fig. 12b.7), and is required to generate the pronounced HREE depletion of A261 (Fig. 12b.2). The fractionation of garnet, as well as the increase in hornblende fractionation of A261 relative to A249, indicates higher water contents (Richards, 2011). Despite the differences in negative Eu and Sr anomalies between the Triassic and Jurassic intrusions, both require 51-53 % plagioclase fractionation. Consequently, the lack of negative Eu and Sr anomalies in the Jurassic samples (A261 and A265) reflects the fractionation of low-Sr and low-Eu plagioclase rather than an absence of plagioclase fractionation. This Sr and Eu compatibility is dominantly controlled by anorthite content (Blundy and Wood, 1991).

Further evidence for an arc setting of the SVFI comes from the U-Pb zircon ages. In contrast to many continental settings (Breitfeld et al., 2019, 2017; Hennig et al., 2017), the SVFI lack inherited zircon ages that would suggest interaction with older basement. The only inherited age found during this study is 245.3±3.2 Ma from the 178.7±1.3 Ma S. LKK. tonalite, A261. This inherited age resembles the older tonalite ages from S. Purut and S. Danum, and thus is likely to be a xenocryst from this older period of magmatism. Consequently, the data presented here provides no evidence for older, continental basement. This contrasts with the conclusion reached from whole rock isotopic compositions of Plio-Pleistocene basalts only 80 km to the SE on the Semporna Peninsula (Fig. 1), which provide evidence for assimilation of an unexposed, much older (possibly even Archaean) continental crust (Fig. 10; Macpherson et al., 2010). However, as the SVFI show no evidence for similar assimilation, any unexposed continental basement is not ubiquitous beneath Sabah.

6.2. Origin of the Sabah ophiolite and mafic arc rocks

The intrusive nature of the Segama Valley Felsic Intrusions demonstrates that the units hosting them must pre-date the Triassic and Jurassic SVFI emplacement age. This extends the age of the Sabah crust back to at least the Triassic. The basaltic sample from S. Purut displays an isotopic affinity to the mantle (Fig. 10) and an arc signature in its trace elements (Fig. 7) comparable to other samples from the Darvel Bay ophiolite (Fig. 1, Omang and Barber, 1996). As noted by Omang and Barber (1996), the mafic ophiolite rocks have tholeiitic compositions (Fig. 7a), ocean floor basalt to low-potassium tholeiite affinity (Fig. 7b and 7c), and relative enrichment of the high field strength elements with relative depletion of the light ion lithophile and LREE (Fig. 9, and Omang and Barber, 1996). These features indicate that the ophiolite was emplaced in a supra-subduction zone extensional basin, potentially ranging from back arc (more MORB affinity) to fore arc (more arc-like affinity).

However, with no field relations to prove an association of the S. Purut basalt with other, deeper stratigraphic units of the ophiolite, and dominantly Cretaceous K-Ar ages for other ophiolite samples, it is hard to prove that the S. Purut basalt is truly “ophiolitic” as opposed to the product of non-ophiolitic arc

magmatism. A Triassic (217 Ma) K-Ar age was obtained for a metagabbro in the Darvel Bay ophiolite (Fig. 1; Omang, 1993), but was rejected on the basis of being much older than the other samples analysed, high in atmospheric Ar^{40}, and low in K. However, in light of the new data, this gabbroic age may need a revaluation; lending support to an ophiolitic origin for the S. Purut basalt. Either way, with regard to tectonic reconstructions, whether the S. Purut basalt represents arc magmatism or is a constituent unit of a supra-subduction zone ophiolite is immaterial, as in both settings the basalt was erupted in at least the Triassic above an active subduction zone. The difference is only whether crustal extension in the overriding plate was sufficient to generate intrabasinal ophiolitic magmatism.

Radiometric and biostratigraphic ages for the ophiolites of Borneo range from Jurassic to Oligocene (198-75 Ma, plus 52 and 33 Ma ages; Coggon et al., 2011; Graves et al., 2000; Hutchison, 2005; Kirk, 1968; Leong, 1974; Omang, 1993; Omang and Barber, 1996; Rangin et al., 1990; Swauger et al., 1995), although all but two gabbro ages (52 and 33 Ma; Graves et al., 2000; Rangin et al., 1990) are Mesozoic (198-75 Ma). In light of our new data, we do not contest the Jurassic to Cretaceous ages, but instead propose that extensional, supra-subduction zone magmatism (including the ophiolite and the SVFI) occurred multiple times during the Mesozoic, focussed along extensional forearc and back-arc basins. This long-lived history of crustal extension and magmatism extended and rifted the continental margin of Sundaland, with disparate unexposed crustal blocks of rifted continental crust only evidenced when assimilated by later magmatism (Cullen et al., 2013; Macpherson et al., 2010). Thus, the Mesozoic history of crustal extension and magmatism was not dissimilar to much of the archipelagic region of SE Asia through the Cenozoic until the present day (Hall, 2012, 1996).

6.3. Nature and extent of the magmatic arc

Based on the field, geochemical, and geochronological evidence presented here, we propose that the SVFI and the Sabah Ophiolite are products of Triassic to Jurassic arc magmatism and supra-subduction zone extension. However, was this arc a continuation of the Paleo-Pacific arc of Sundaland, or an accreted terrane?

Various techniques can differentiate autochthonous and allochthonous terranes (Burton-Johnson and Riley, 2015). However, with no paleomagnetic data or geochemical evidence for crustal assimilation in the SVFI or host ophiolite, the only available methodology to trace the origin of the Sabah arc is to compare the timing of SVFI magmatism with regional magmatic events and detrital zircon geochronology. The Paleo-Pacific arc of Sundaland experienced a peak in magmatic activity in the Triassic, including SE China, Hainan Island, Vietnam, the Malaysian Peninsula, and West Borneo (Breitfeld et al., 2017; Fyhn et al., 2016). Comparing the SVFI U-Pb data with outcrops along the Paleo-Pacific arc shows a close agreement between the Triassic SVFI ages and a flare-up in igneous magmatism in the NW Schwaner Mountains of west Kalimantan (Fig. 13c; Hennig et al., 2017; Setiawan et al., 2013) and the plutons of Singapore and the east coast of the Malay Peninsula (Fig. 13b; Liew, 1983; Oliver et al., 2014). This peak is also recorded in the detrital zircons of the Triassic Sadong Formation and Cretaceous Pedawan Formation of Sarawak (Fig. 13d and 13e; Breitfeld et al., 2017). Similarly, the Jurassic SVFI ages are contemporaneous with another peak in Schwaner Mountains intrusive magmatism (Fig. 13c; Hennig et al., 2017) and the onset of another peak in detrital zircon ages in the Cretaceous Pedawan Formation (Fig. 13d; Breitfeld et al., 2017). With this close agreement in the geochronology from both the magmatic and detrital record, we propose that the Triassic and Jurassic arc of Sabah is an autochthonous continuation of the Sundaland Paleo-Pacific arc rather than an accreted allochthonous terrane.

Previous tectonic reconstructions of Borneo (Fig. 14a; Breitfeld et al., 2017; Hall, 2017; Hennig et al., 2017) have assumed an absence of autochthonous pre-Cretaceous crust beneath Sabah, and have suggested that the region developed as a result of the accretion of allochthonous crust in the Cretaceous (the Inner Banda Block; Hennig et al., 2017, 2016). Our identification of the Paleo-Pacific arc continuing from Kalimantan to Sabah during the Triassic and Jurassic challenges this model, developing Sabah *in-situ* through autochthonous growth through supra-subduction zone magmatism, and extending the arc and the region of early-Mesozoic crust in Borneo to the south (Fig. 14b). However, the Borneo crust would have been less extensive than it is today, as an extensional setting is required for the genesis of the Mesozoic supra-subduction zone

ophiolites and Mesozoic-Cenozoic basins, representing a protracted history of supra-subduction zone extension throughout the Mesozoic and Cenozoic. The evidence for, and distance by which the granitoids and their host rocks may have been transported by extensional or strike-slip tectonics may be potentially constrainable by paleomagnetic analysis.

7. Conclusions

The tonalitic outcrops of the Segama Valley Felsic Intrusions are Triassic and Jurassic in age and post-date the supra-subduction zone rocks into which they are intruded These rocks are not windows or partial melts of an unexposed continental basement beneath Borneo. They represent mantle-derived arc magmatism in a continuation of the Mesozoic Paleo-Pacific continental arc that extended through SW Borneo, Sundaland, Vietnam, and SE China. Their age and intrusive nature provide a minimum estimate for the formation of the Sabah ophiolite, which must be of at least Triassic age. We propose that emplacement of the Sabah ophiolite continued over a protracted period into the Cretaceous, in an extensional, supra-subduction zone setting.

9. Acknowledgements

NERC supported this study through a PhD studentship to AB-J. We thank Richard Hinton for his analytical support in acquiring the U-Pb data, and Robert Hall, Mike Cottam, Juliane Hennig and the SE Asia Research Group at Royal Holloway for their support throughout this project and comments on this manuscript. We thank A.J. Barber and anonymous reviewer for their helpful and positive reviews, and Sanghoon Kwon for their work as our editor.

References

Balaguru, A., 2001. Tectonic evolution and sedimentation of the southern Sabah basins, Malaysia (PhD Thesis). Royal Holloway, University of London.

Black, L.P., Kamo, S.L., Allen, C.M., Davis, D.W., Aleinikoff, J.N., Valley, J.W., Mundil, R., Campbell, I.H., Korsch, R.J., Williams, I.S., 2004. Improved 206Pb/238U microprobe geochronology by the monitoring of a trace-element-related matrix effect; SHRIMP, ID–TIMS, ELA–ICP–MS and oxygen isotope documentation for a series of zircon standards. Chem. Geol. 205, 115–140.

Blundy, J.D., Wood, B.J., 1991. Crystal-chemical controls on the partitioning of Sr and Ba between plagioclase feldspar, silicate melts, and hydrothermal solutions. Geochim. Cosmochim. Acta 55, 193–209.

Bouvier, A., Vervoort, J.D., Patchett, P.J., 2008. The Lu–Hf and Sm–Nd isotopic composition of CHUR: constraints from unequilibrated chondrites and implications for the bulk composition of terrestrial planets. Earth Planet. Sci. Lett. 273, 48–57.

Breitfeld, H.T., Hall, R., Galin, T., Forster, M.A., BouDagher-Fadel, M.K., 2017. A Triassic to Cretaceous Sundaland–Pacific subduction margin in West Sarawak, Borneo. Tectonophysics 694, 35–56.

Breitfeld, H.T., Macpherson, C., Hall, R., Thirlwall, M., Ottley, C.J., Hennig-Breitfeld, J., 2019. Adakites without a slab: Remelting of hydrous basalt in the crust and shallow mantle of Borneo to produce the Miocene Sintang Suite and Bau Suite magmatism of West Sarawak. Lithos 100–121.

Burton-Johnson, A., Macpherson, C.G., Ottley, C.J., Nowell, G.M., Boyce, A.J., 2019. Generation of the Mt Kinabalu granite by crustal contamination of intraplate magma modelled by Equilibrated Major Element Assimilation with Fractional Crystallisation (EME-AFC). J. Petrol. 60, 1461–1487.

Burton-Johnson, A., Riley, T.R., 2015. Autochthonous v. accreted terrane development of continental margins: a revised in situ tectonic history of the Antarctic Peninsula. J. Geol. Soc. 172, 822–835.

Charlier, B.L. a., Ginibre, C., Morgan, D., Nowell, G.M., Pearson, D.G., Davidson, J.P., Ottley, C.J., 2006. Methods for the microsampling and high-precision analysis of strontium and rubidium isotopes at single crystal scale for petrological and geochronological applications. Chem. Geol. 232, 114–133. https://doi.org/10.1016/j.chemgeo.2006.02.015

Coggon, J.A., Nowell, G.M., Pearson, D.G., Parman, S.W., 2011. Application of the 190Pt-186Os isotope system to dating platinum mineralization and ophiolite formation: an example from the Meratus Mountains, Borneo. Econ. Geol. 106, 93–117.

Collenette, P., 1965. The geology and mineral resources of the Pensiangan and Upper Kinabatangan area, Sabah. Malays. Geol. Surv. Borneo Reg. Mem. 12, 150.

Cullen, A., Macpherson, C., Taib, N.I., Burton-Johnson, A., Geist, D., Spell, T., Banda, R.M., 2013. Age and petrology of the Usun Apau and Linau Balui volcanics: Windows to central Borneo's interior. J. Asian Earth Sci. 76, 372–388. https://doi.org/10.1016/j.jseaes.2013.05.003

DePaolo, D.J., 1981. Trace element and isotopic effects of combined wallrock assimilation and fractional crystallization. Earth Planet. Sci. Lett. 53, 189–202.

DePaolo, D.J., Wasserburg, G.J., 1979. Petrogenetic mixing models and Nd-Sr isotopic patterns. Geochim. Cosmochim. Acta 43, 615–627.

Eiler, J.M., 2001. Oxygen isotope variations of basaltic lavas and upper mantle rocks. Rev. Mineral. Geochem. 43, 319–364.

Faure, G., 1986. Principles of isotope geology, 2nd ed. Wiley, Chichester, UK.

Fyhn, M.B., Green, P.F., Bergman, S.C., Van Itterbeeck, J., Tri, T.V., Dien, P.T., Abatzis, I., Thomsen, T.B., Chea, S., Pedersen, S.A., 2016. Cenozoic deformation and exhumation of the Kampot Fold Belt and implications for south Indochina tectonics. J. Geophys. Res. Solid Earth 121, 5278–5307.

Galer, S.J.G., 1997. Optimal triple spiking for high precision lead isotope ratio determination. Terra Nova 9, 441.

Gill, R., 1997. Modern Analytical Geochemistry: an introduction to quantitative chemical analysis techniques for Earth, environmental and materials scientists. Routledge, London, UK.

Graves, J.E., Hutchison, C.S., Bergman, S.C., Swauger, D.A., 2000. Age and MORB geochemistry of the Sabah ophiolite basement. Geol. Soc. Malays. Bull. 44, 151–158.

Hall, R., 2017. Southeast Asia: new views of the geology of the Malay Archipelago. Annu. Rev. Earth Planet. Sci. 45, 331–358.

Hall, R., 2012. Late Jurassic–Cenozoic reconstructions of the Indonesian region and the Indian Ocean. Tectonophysics 570–571, 1–41. https://doi.org/10.1016/j.tecto.2012.04.021

Hall, R., 1996. Reconstructing Cenozoic SE Asia, in: Hall, R., Blundell, D.J. (Eds.), Tectonic Evolution of SE Asia, Geological Society, London, Special Publications. pp. 153–184.

Hall, R., Wilson, M.E.J., 2000. Neogene sutures in eastern Indonesia. J. Asian Earth Sci. 18, 781–808.

Hennig, J., Breitfeld, H.T., Hall, R., Nugraha, A.S., 2017. The Mesozoic tectono-magmatic evolution at the Paleo-Pacific subduction zone in West Borneo. Gondwana Res. 48, 292–310.

Hennig, J., Hall, R., Armstrong, R.A., 2016. U-Pb zircon geochronology of rocks from west Central Sulawesi, Indonesia: Extension-related metamorphism and magmatism during the early stages of mountain building. Gondwana Res. 32, 41–63.

Holt, R., 1998. The Gravity Field of Sundaland: Acquisition, Assessment and Interpretation (PhD Thesis). Birkbeck, University of London.

Hutchison, C., 2000. A Miocene collisional belt in north Borneo: uplift mechanism and isostatic adjustment quantified by thermochronology. J. Geol. Soc. 157, 783–793.

Hutchison, C., 1975. Ophiolite in southeast Asia. Geol. Soc. Am. Bull. 86, 797–806. https://doi.org/10.1130/0016-7606(1975)86<797

Hutchison, C.S., 2005. Geology of North-West Borneo: Sarawak, Brunei and Sabah. Elsevier, Amsterdam, The Netherlands.

Hutchison, C.S., 1996. The “Rajang accretionary prism” and “Lupar Line” problem of Borneo. Geol. Soc. Lond. Spec. Publ. 106, 247–261. https://doi.org/10.1144/GSL.SP.1996.106.01.16

Hutchison, C.S., 1988. Stratigraphic-tectonic model for eastern Borneo. Geol. Soc. Malays. Bull. 22, 135–151.

Irvine, T.N.J., Baragar, W.R.A., 1971. A guide to the chemical classification of the common volcanic rocks. Can. J. Earth Sci. 8, 523–548.

Jasin, B., 1992. Significance of radiolarian cherts from the Chert-Spilite Formation, Telupid, Sabah. Sabah Geol. Soc. Malays. Bull. 31, 67–83.

Kelly, N.M., Hinton, R.W., Harley, S.L., Appleby, S.K., 2008. New SIMS U–Pb zircon ages from the Langavat Belt, South Harris, NW Scotland: implications for the Lewisian terrane model. J. Geol. Soc. 165, 967–981.

Kirk, H.J.C., 1968. The igneous rocks of Sarawak and Sabah. Geol. Surv. Borneo Reg. Malays. Bull. 5, 201.

Lehnert, K., Su, Y., Langmuir, C.H., Sarbas, B., Nohl, U., 2000. A global geochemical database structure for rocks. Geochem. Geophys. Geosystems 1.

Leong, K.M., 2017. Review of 50-Years (1966–2016) Debate on Age of Sabah Crystalline Basement Granitic Rocks: Are the Granitic Rocks in Upper Segama Sabah Fragments of Supercontinent Pangaea? War. Geol. 43, 223–224.

Leong, K.M., 1998. Sabah crystalline basement:"Spurious" radiometric ages? Continental. War. Geol. Geol. Soc. Malays. Newsl. 24, 5–8.

Leong, K.M., 1974. The geology and mineral resources of the Upper Segama Valley and Darvel Bay area, Sabah, Malaysia. Geol. Surv. Malays. Mem. 4.

Liew, T.C., 1983. Petrogenesis of the Peninsular Malaysian granitoid batholiths (PhD Thesis). Australian National University, Canberra, Australia.

Ludwig, K.R., 2003. User Manual for Isoplot 3.00: A Geochronological Toolkit for Microsoft Excel. Berkeley Geochronol. Cent. Spec. Publ. 4, 70.

Macpherson, C.G., Chiang, K.K., Hall, R., Nowell, G.M., Castillo, P.R., Thirlwall, M.F., 2010. Plio-Pleistocene intra-plate magmatism from the southern Sulu Arc, Semporna peninsula, Sabah, Borneo: Implications for high-Nb basalt in subduction zones. J. Volcanol. Geotherm. Res. 190, 25–38. https://doi.org/10.1016/j.jvolgeores.2009.11.004

Macpherson, C.G., Hilton, D.R., Mattey, D.P., Sinton, J.M., 2000. Evidence for an 18O-depleted mantle plume from contrasting 18O/16O ratios of back-arc lavas from the Manus Basin and Mariana Trough. Earth Planet. Sci. Lett. 176, 171–183.

Macpherson, C.G., Mattey, D.P., 1998. Oxygen isotope variations in Lau Basin lavas. Chem. Geol. 144, 177–194. https://doi.org/10.1016/S0009-2541(97)00130-7

Mattey, D., Lowry, D., Macpherson, C., 1994. Oxygen isotope composition of mantle peridotite. Earth Planet. Sci. Lett. 128, 231–241. https://doi.org/10.1016/0012-821X(94)90147-3

Metcalfe, I., 2011. Tectonic framework and Phanerozoic evolution of Sundaland. Gondwana Res. 19, 3–21. https://doi.org/10.1016/j.gr.2010.02.016

Milsom, J., Holt, R., Hutchison, C.S., Bergman, S.C., Swauger, D.A., Graves, J.E., 2001. Discussion of a Miocene collisional belt in north Borneo: uplift mechanism and isostatic adjustment quantified by thermochronology: Journal, Vol. 157, 2000, 783–793. J. Geol. Soc. 158, 396–400.

Moss, S.J., 1998. Embaluh Group turbidites in Kalimantan: evolution of a remnant oceanic basin in Borneo during the Late Cretaceous to Palaeogene. J. Geol. Soc. 155, 509–524. https://doi.org/10.1144/gsjgs.155.3.0509

Nowell, G., Parrish, R.R., 2001. Simultaneous acquisition of isotope compositions and parent/daughter ratios by non-isotope dilution-mode plasma ionisation muti-colector mass spectrometry (PIMMS), in: Holland, G., Tanner, S.D. (Eds.), Plasma Source Mass Spectrometry: The New Millennium, Royal Society of Chemistry, Special Publications. pp. 298–310.

Oliver, G., Zaw, K., Hotson, M., Meffre, S., Manka, T., 2014. U–Pb zircon geochronology of Early Permian to Late Triassic rocks from Singapore and Johor: A plate tectonic reinterpretation. Gondwana Res. 26, 132–143.

Omang, S., 1993. Petrology, geochemistry and structural geology of the Darvel Bay Ophiolite, Sabah, Malaysia (PhD Thesis). University of London.

Omang, S.A.K., Barber, A.J., 1996. Origin and tectonic significance of the metamorphic rocks associated with the Darvel Bay Ophiolite, Sabah, Malaysia. Geol. Soc. Lond. Spec. Publ. 106, 263–279. https://doi.org/10.1144/GSL.SP.1996.106.01.17

Paton, C., Hellstrom, J., Paul, B., Woodhead, J., Hergt, J., 2011. Iolite: Freeware for the visualisation and processing of mass spectrometric data. J. Anal. At. Spectrom. 26, 2508–2518.

Pearce, J.A., 2003. Supra-subduction zone ophiolites: the search for modern analogues. Spec. Pap.-Geol. Soc. Am. 269–294.

Pearce, J.A., Cann, J.R., 1973. Tectonic setting of basic volcanic rocks determined using trace element analyses. Earth Planet. Sci. Lett. 19, 290–300.

Pearce, J.A., Harris, N.B.W., Tindle, a. G., 1984. Trace Element Discrimination Diagrams for the Tectonic Interpretation of Granitic Rocks. J. Petrol. 25, 956–983. https://doi.org/10.1093/petrology/25.4.956

Rangin, C., Bellon, H., Benard, F., Letouzey, J., Muller, C., Sanudin, T., 1990. Neogene arc-continent collision in Sabah, Northern Borneo (Malaysia). Tectonophysics 183, 305–319. https://doi.org/10.1016/0040-1951(90)90423-6

Rangin, C., Silver, E.A., 1990. Geological setting of the Celebes and Sulu Seas. Proc. Ocean Drill. Program Initial Rep. 124, 35–42.

Reinhard, M., Wenk, E., 1951. Geology of the Colony of North Borneo. Geol. Surv. Dep. Br. Territ. Borneo Bull. 1, 160.

Richards, J.P., 2011. High Sr/Y arc magmas and porphyry Cu$\pm$Mo$\pm$Au deposits: just add water. Econ. Geol. 106, 1075–1081.

Royse, K.R., Kempton, P.D., Darbyshire, D.P.F., 1998. Procedure for the analysis of rubidium–strontium and samarium–neodymium isotopes at the NERC Isotope Geosciences Laboratory. NIGL Rep. Ser. 121, 28.

Setiawan, N.I., Osanai, Y., Nakano, N., Adachi, T., Setiadji, L.D., Wahyudiono, J., 2013. Late Triassic metatonalite from the Schwaner Mountains in West Kalimantan and its contribution to sedimentary provenance in the Sundaland. Ber. Sedimentol. 12, 4–12.

Söderlund, U., Patchett, P.J., Vervoort, J.D., Isachsen, C.E., 2004. The 176 Lu decay constant determined by Lu–Hf and U–Pb isotope systematics of Precambrian mafic intrusions. Earth Planet. Sci. Lett. 219, 311–324.

Steinshouer, D.W., Qiang, J., McCabe, P.J., Ryder, R.T., 1999. Maps showing geology, oil and gas fields and geologic provinces of the Asia Pacific Region: U.S. Geological Survey Open-File Report OF-97–470F.

Sun, S. -s., McDonough, W.F., 1989. Chemical and isotopic systematics of oceanic basalts: implications for mantle composition and processes. Geol. Soc. Lond. Spec. Publ. 42, 313–345. https://doi.org/10.1144/GSL.SP.1989.042.01.19

Swauger, D.A., Bergman, S.C., Graves, J.E., Hutchison, C.S., Surat, T., Morillo, A.P., Benavidez, J.J., Pagado, E.S., 1995. Tertiary stratigraphic, tectonic, and thermal history of Sabah, Malaysia: results of a 10 day reconnaissance field study and laboratory analyses. ARCO Int. Oil Gas Co Unpubl. Rep. TRS 95-0036.

Taylor, B., Hayes, D.E., 1983. Origin and history of the South China Sea basin, in: Hayes, D.E. (Ed.), The Tectonic and Geologic Evolution of Southeast Asian Seas and Islands: Part 2, American Geophysical Union, Geophysical

Monographs Series. American Geophysical Union, Washington D.C., USA, pp. 23–56.

Thirlwall, M., 1991. Long-term reproducibility of multicollector Sr and Nd isotope ratio analysis. Chem. Geol. Isot. Geosci. Sect. 94, 85–104.

Tongkul, F., 1994. The geology of Northern Sabah, Malaysia: its relationship to the opening of the South China Sea Basin. Tectonophysics 235, 131–147.

Tongkul, F., 1991. Tectonic evolution of Sabah, Malaysia. J. Southeast Asian Earth Sci. 6, 395–405.

Valley, J., 2003. Oxygen isotopes in zircon, in: Hanchar, J.M., Hoskin, P.W.O. (Eds.), Zircon, Reviews in Mineralogy and Geochemistry. The Mineralogical Society of America, Washington DC, USA, pp. 343–385.

van Hattum, M.W., Hall, R., Pickard, A.L., Nichols, G.J., 2006. Southeast Asian sediments not from Asia: Provenance and geochronology of north Borneo sandstones. Geology 34, 589–592.

Wakita, K., Miyazaki, K., Zulkarnain, I., Sopaheluwakan, J., Sanyoto, P., 1998. Tectonic implications of new age data for the Meratus Complex of south Kalimantan, Indonesia. Isl. Arc 7, 202–222.

Whitehouse, M.J., Nemchin, A.A., 2009. High precision, high accuracy measurement of oxygen isotopes in a large lunar zircon by SIMS. Chem. Geol. 261, 32–42.

Wiedenbeck, M., Alle, P., Corfu, F., Griffin, W.L., Meier, M., Oberli, F. v, Quadt, A. von, Roddick, J.C., Spiegel, W., 1995. Three natural zircon standards for U-Th-Pb, Lu-Hf, trace element and REE analyses. Geostand. Newsl. 19, 1–23.

Wiedenbeck, M., Hanchar, J.M., Peck, W.H., Sylvester, P., Valley, J., Whitehouse, M., Kronz, A., Morishita, Y., Nasdala, L., Fiebig, J., 2004. Further characterisation of the 91500 zircon crystal. Geostand. Geoanalytical Res. 28, 9–39.

Williams, P.R., Johnston, C.R., Almond, R.A., Simamora, W.H., 1988. Late Cretaceous to early Tertiary structural elements of West Kalimantan. Tectonophysics 148, 279–297.

Woodhead, J.D., Hergt, J.M., 2005. A preliminary appraisal of seven natural zircon reference materials for in situ Hf isotope determination. Geostand. Geoanalytical Res. 29, 183–195.

Journal Pre-proof

Figure Captions

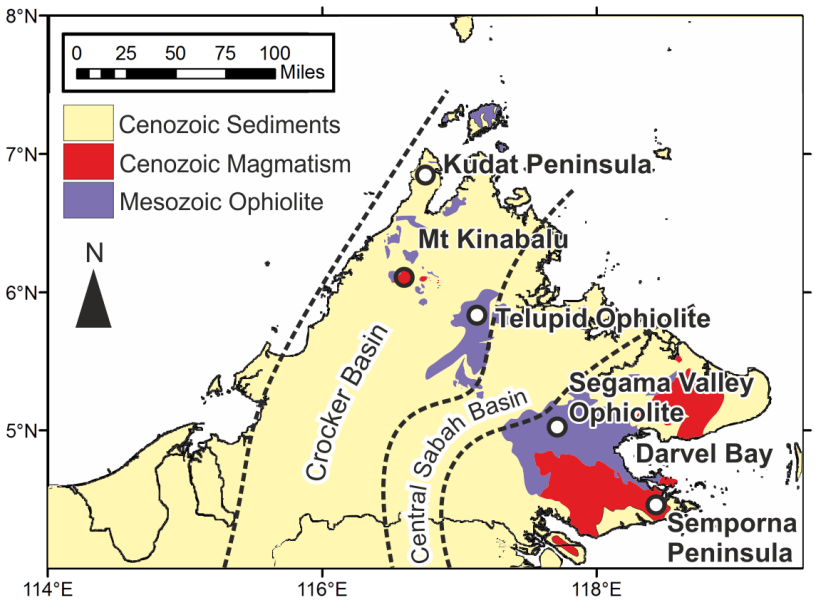

Fig. 1. Regional map and simplified geological map of Sabah, showing the distribution of Mesozoic ophiolite outcrops, Cenozoic magmatism, and sedimentary basins (Kirk, 1968, Hutchison, 2005).

Journal Pre-proof

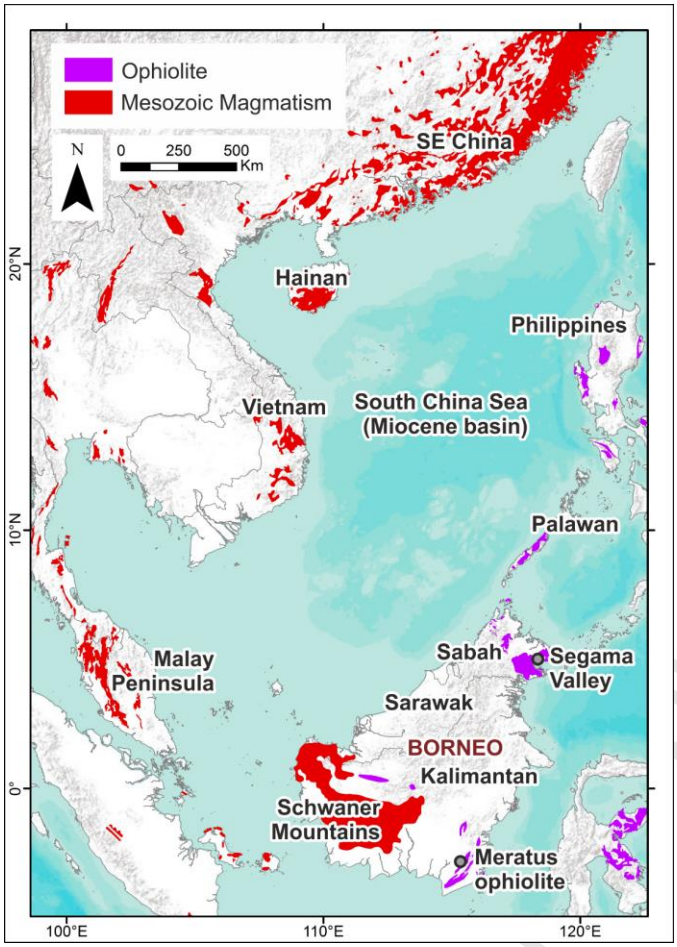

Fig. 2. Regional distribution of ophiolites and Mesozoic magmatism in SE Asia and the South China Sea (Hutchison, 1975, 2005; Kirk, 1968; Moss, 1998; Steinshouer et al., 1999; Wakita et al., 1998).

Journal Pre-proof

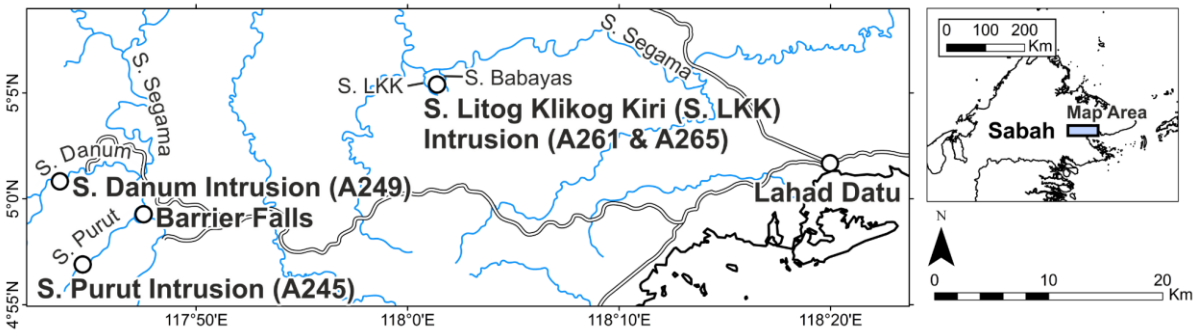

Fig. 3. Regional map of the Segama Valley area, Sabah, and sample locations of the Segama Valley Felsic Intrusions.

Journal Pre-proof

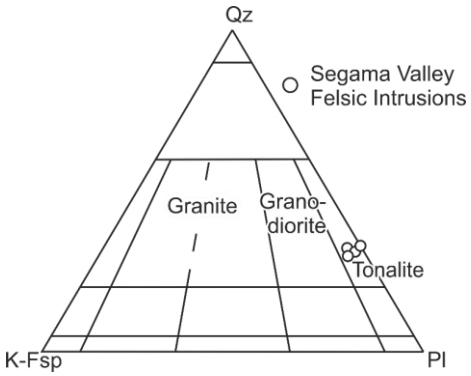

Fig. 4. IUGS QAP (Streckeisen, 1976) classifications of the Segama Valley Felsic Intrusions. Sections stained for plagioclase and K-Feldspar. Point counting based on 300 points per sample.

Journal Pre-proof

Fig. 5. a) Xenolith of basaltic country rock within the S. Purut tonalite near the intrusive contact. b) Downstream end of the Danum Gorge, showing the intrusive contact of the S. Danum tonalite intrusion with the sedimentary country rock. c) Contact margin between the S. Danum intrusion and sedimentary country rock. 71 cm long sledgehammer for scale.

Journal Pre-proof

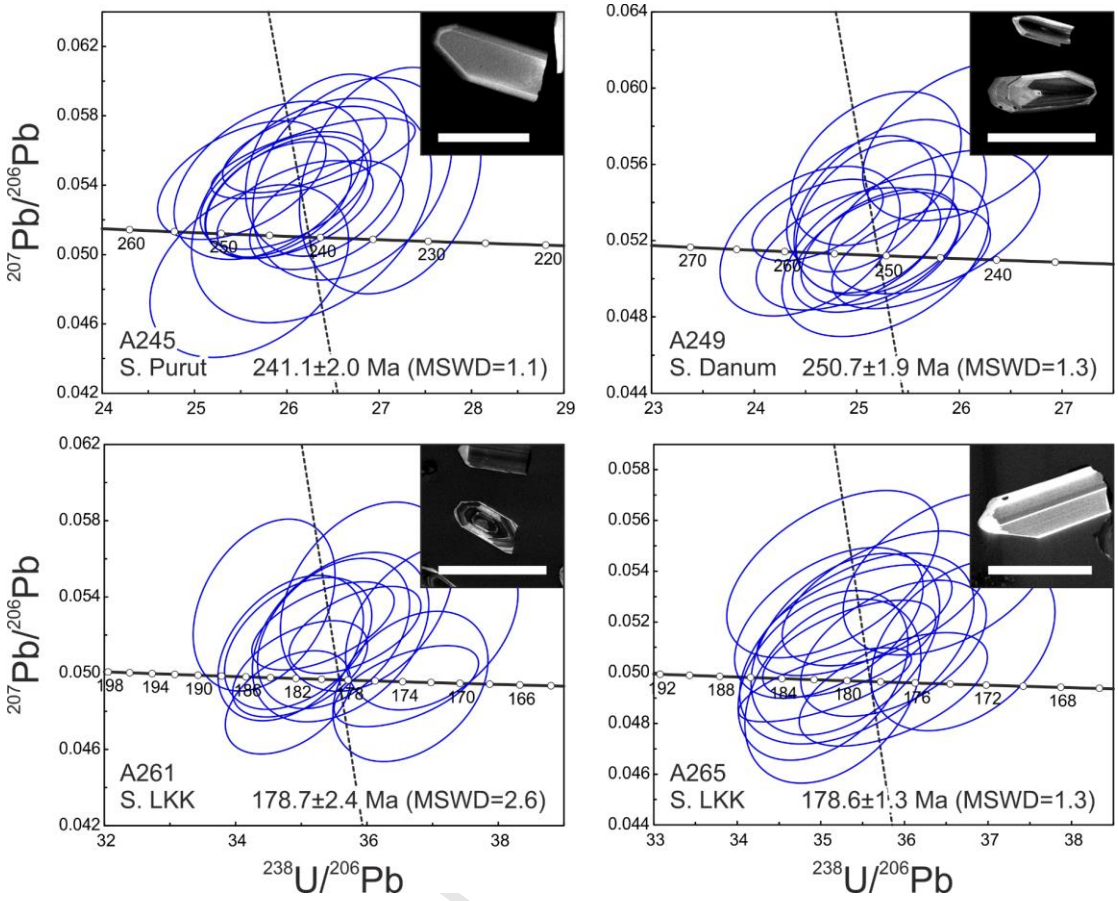

Fig. 6. Concordia diagrams of the zircon U-Pb dating of the Segama Valley Felsic Intrusions. Error ellipses denote 2 sigma. Uncertainties in calculated age are the 95% confidence limit. Inlays show representative cathodoluminescence images of the analysed zircons from each sample, with 100 μm scale bars. MSWD – mean square of weighted deviates.

Journal

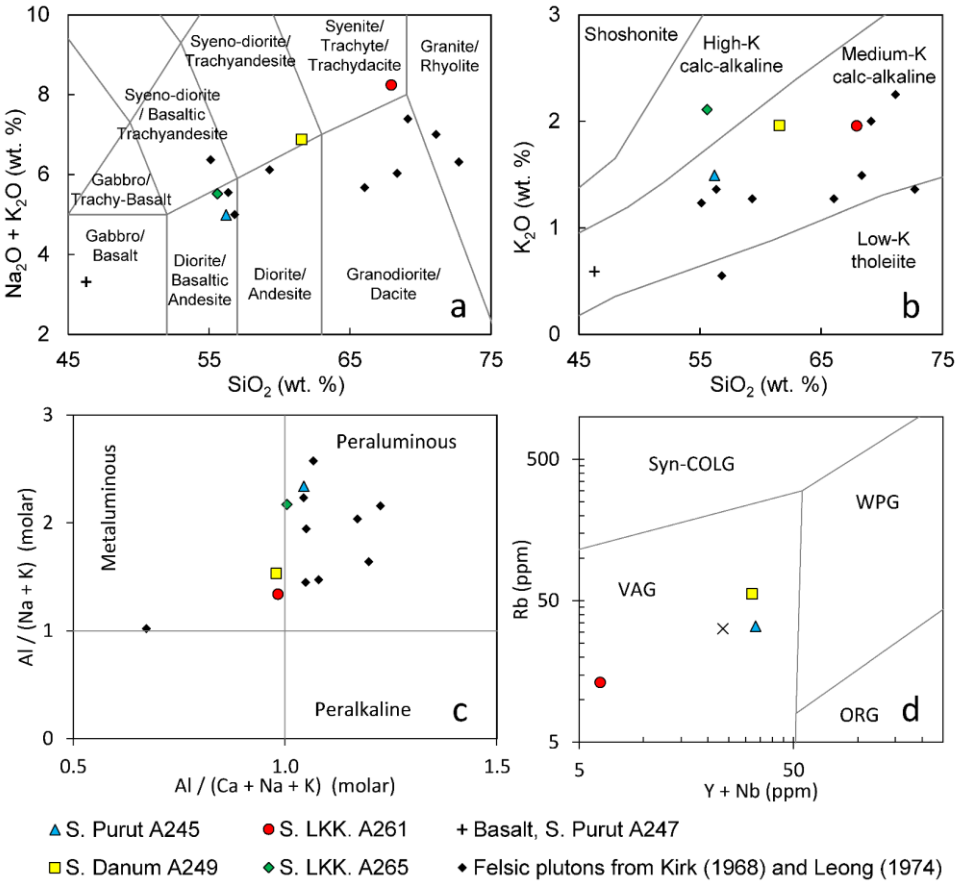

Fig. 7. a), b), and c) Major element classification diagrams for the Segama Valley Felsic Intrusions. Felsic plutons from the Segama Valley from Kirk (1968) and Leong (1974) plotted for comparison. Classification fields from Le Maitre et al. (1989), Rickwood (1989). d) Tectonic discrimination diagram of the Segama Valley Felsic Intrusions (Pearce et al., 1984). ORG – Ocean ridge granitoids; Syn-COLG – Syn-collisional granitoids; VAG – Volcanic arc granitoids; WPG – Within-plate granitoids.

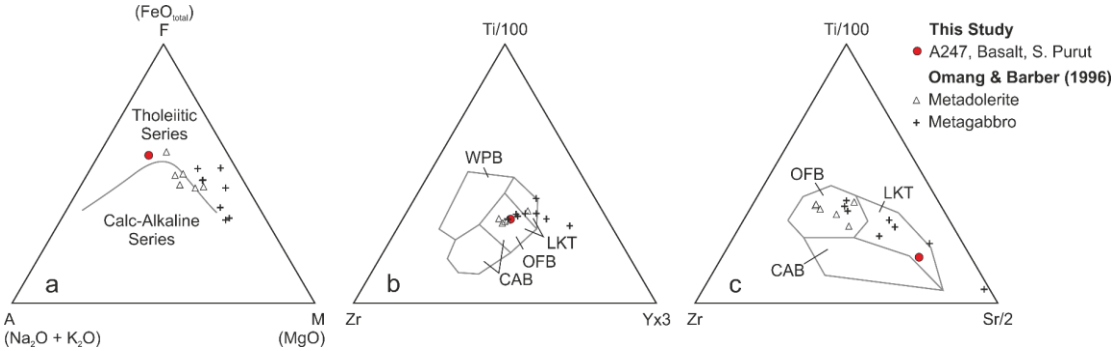

Fig. 8. Geochemical discrimination diagrams for the mafic rocks of the Segama Valley and Darvel Bay ophiolite (this study and Omang and Barber, 1996). a) Delineation of the tholeiitic and calc-alkaline series (Irvine and Baragar, 1971). b) and c) Tectonic discrimination diagrams (Pearce and Cann, 1973). CAB – Calc-alkaline basalt; LKT – Low-potassium tholeiite; OFB – Ocean floor basalt; WPB – Within plate basalt.

Journal Pre-proof

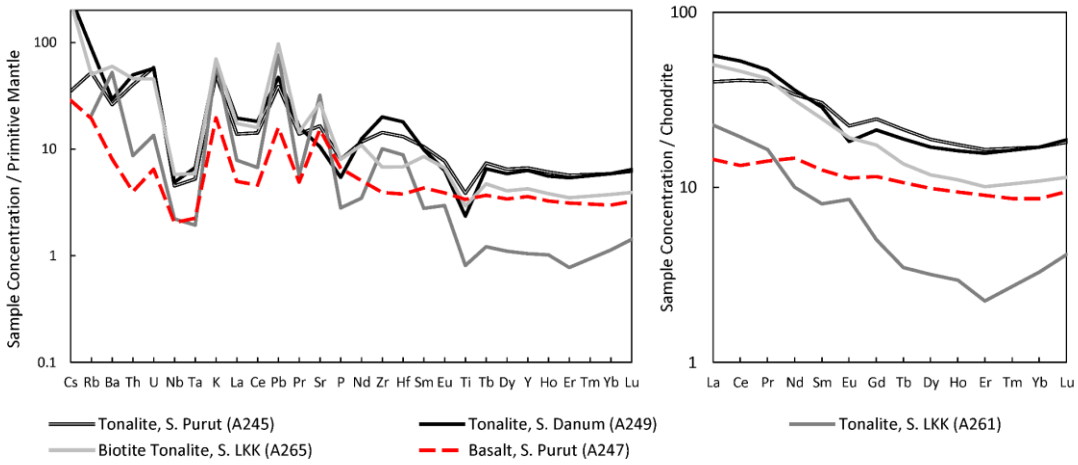

Fig. 9. Normalised multi-element plots for the felsic Segama Valley Felsic Intrusions. Normalising values and N-MORB composition from Sun and McDonough (1989).

Journal Pre-proof

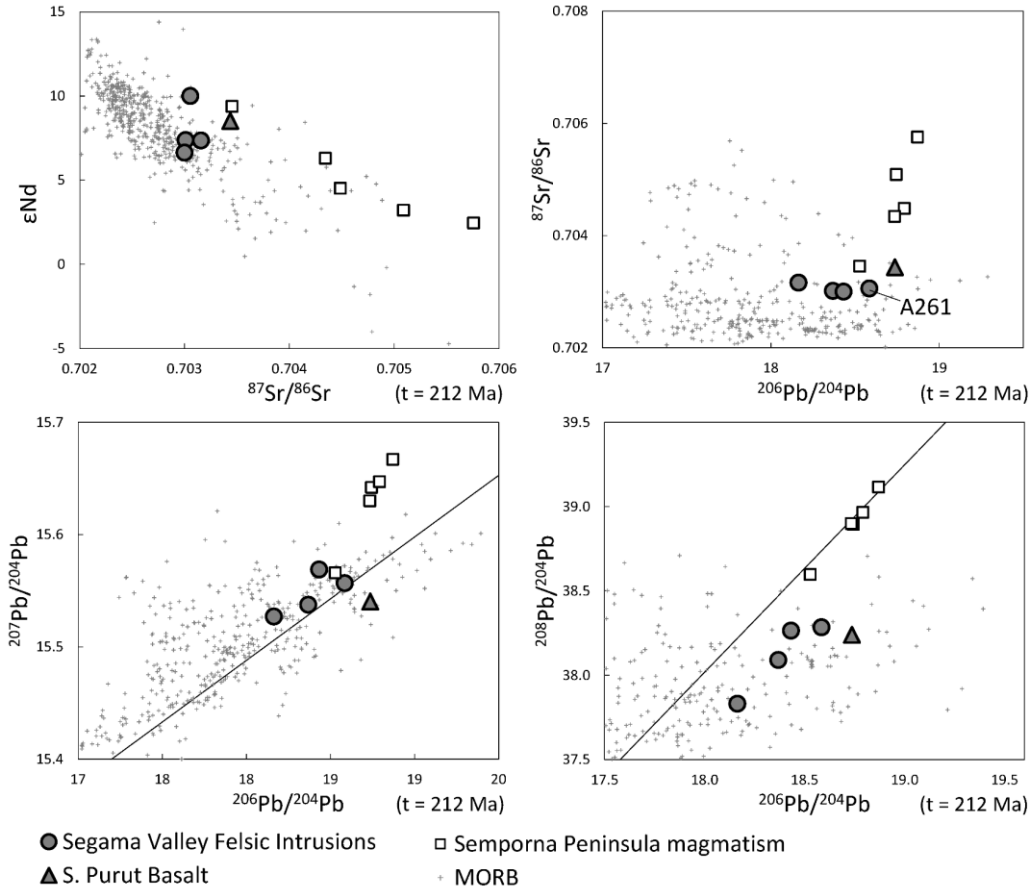

Fig. 10. Comparison of isotopic signatures of the Segama Valley Felsic Intrusions with values for spreading ridge basalts (shaded area) of the Indian, Pacific and Atlantic Oceans (data from PetDB) and the Plio-Pleistocene basalts and basaltic andesites of the Semporna Peninsula (Fig. 1; Macpherson et al., 2010). Isotopic values corrected to the mean U-Pb zircon age of the four SVFI samples (Fig. 6, 212 Ma).

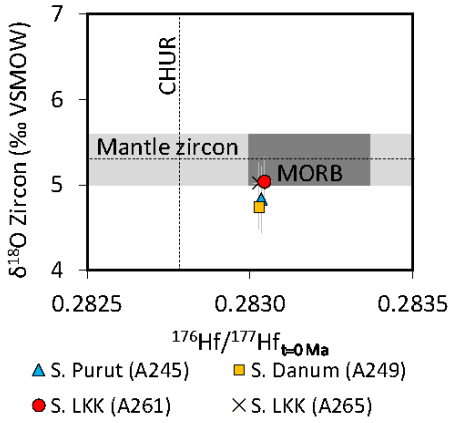

Fig. 11. Zircon Hf and $\delta^{18}O$ values of the Segama Valley Felsic Intrusions (for the same samples analysed for U-Pb, Fig. 6). Dark grey box indicates the 2SD range of MORB Hf isotope compositions from PetDB for the Atlantic, Pacific, and Indian Ocean spreading centres (Lehnert et al., 2000), for which a mantle $\delta^{18}O$ composition is assumed. $\delta^{18}O$ range for zircon in equilibrium with the mantle (5.3±0.3‰) from Valley (2003). CHUR $^{176}Hf/^{177}Hf$ value from Bouvier et al. (2008).

Journal Pre-proof

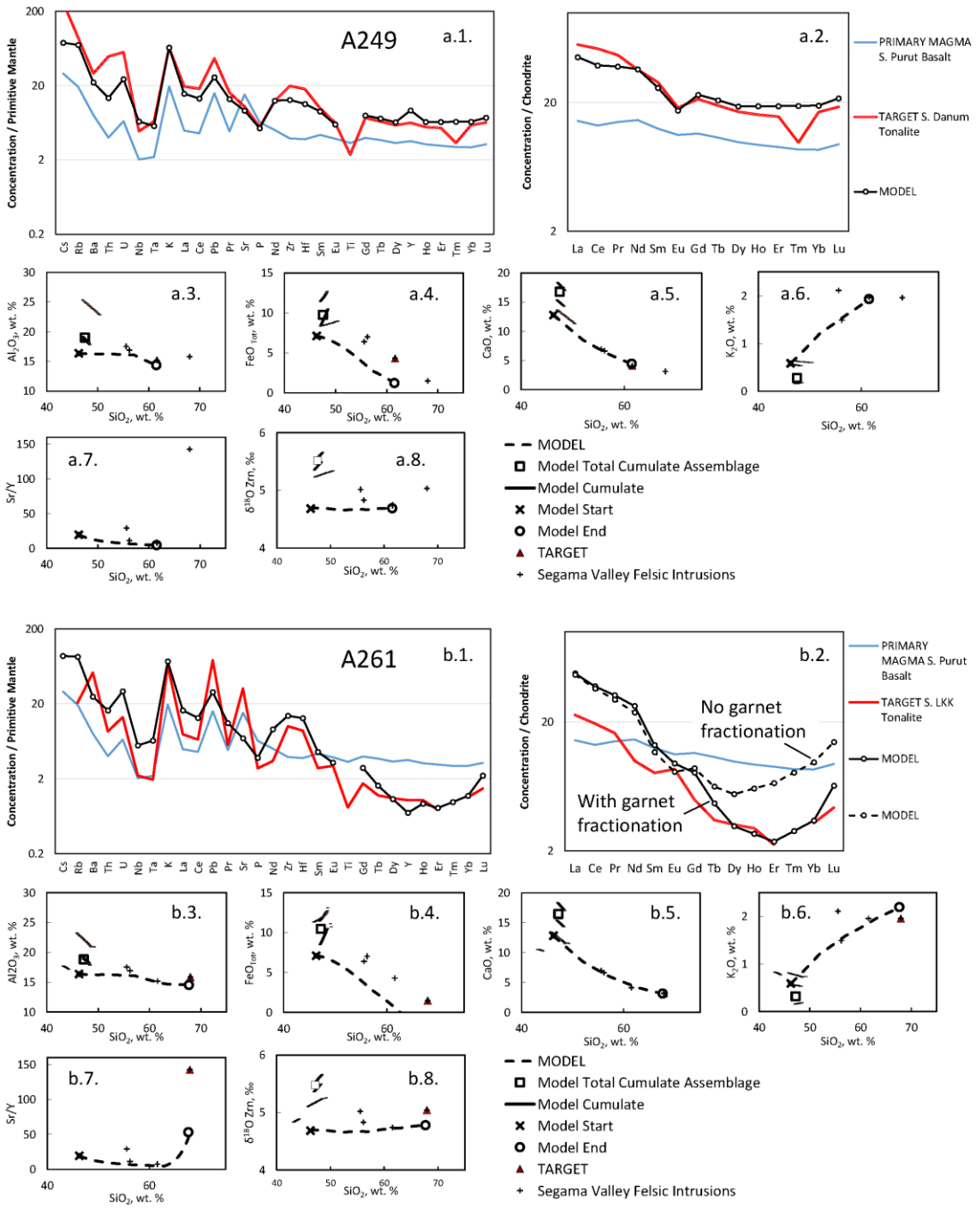

Fig. 12. Comparison of analysed compositions (isotopes, trace elements and selected major elements) and EME-AFC modelling of the derivation of the A249 and A261 tonalites from the A247 basalt. Comparison of modelling of A261 with and without garnet fractionation when melt SiO_2 > 63 wt. % shown in 'b.2'. Cumulate plots a.8. and b.8. are whole rock values. Normalising values from Sun and McDonough (1989).

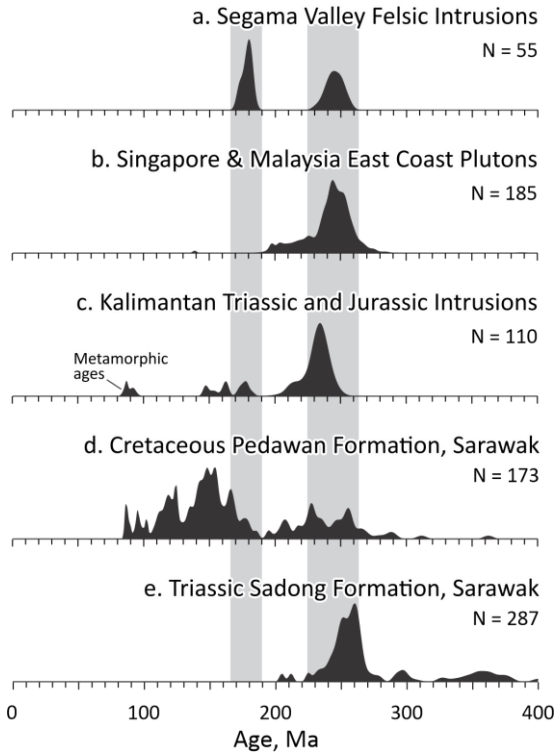

Fig. 13. Probability density plots of 0-400 Ma $^{206}Pb/^{238}U$ zircon ages from a) the Segama Valley Felsic Intrusions; b) the Triassic and Jurassic plutons of Singapore and the east coast of Peninsula Malaysia (Liew, 1983; Oliver et al., 2014); c) the Schwaner Mountains, West Kalimantan (Hennig et al., 2017; Setiawan et al., 2013); and detrital zircon ages from the d) Pedawan and e) Sadong Formations of Sarawak, NW Borneo (Breitfeld et al., 2017).

Journal Pre-proof

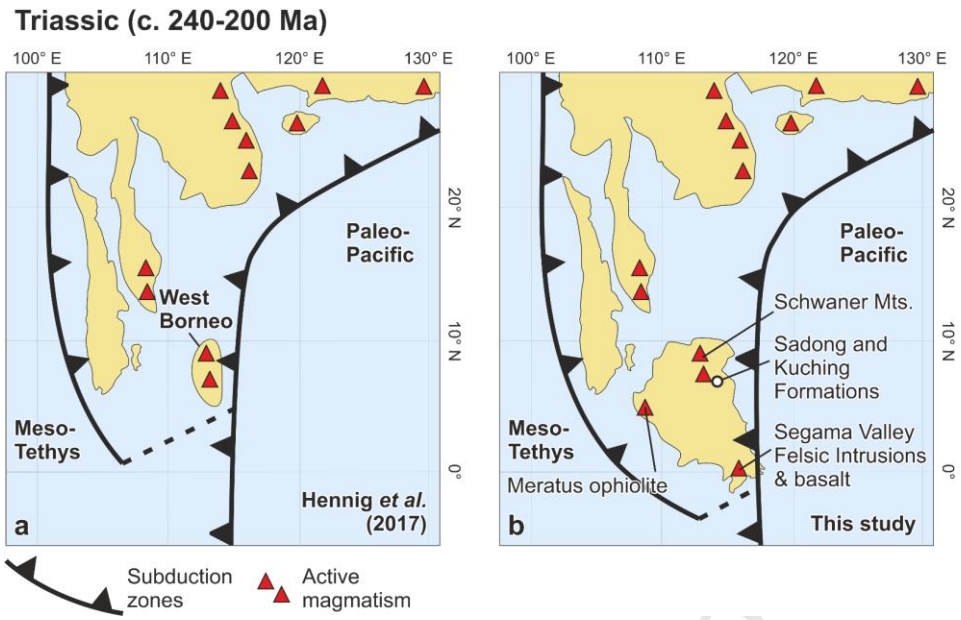

Fig. 14. Schematic tectonic reconstructions of SE Asia in the Triassic to show the possible origin of Segama Valley intrusions. a) Reconstruction of Hennig et al. (2017) with active magmatism from Breitfeld et al. (2017). b) Modified reconstruction of Hennig et al. (2017) incorporating the data presented in this study. The Paleo-Pacific arc is extended into Sabah, with a consequent requirement for incorporation of much of Borneo. Other Triassic or earliest Jurassic outcrops in Borneo include the Schwaner Mountains of West Borneo (Hennig et al., 2017; Williams et al., 1988), the 197.8 to 110 Ma Meratus ophiolite of Kalimantan (Coggon et al., 2011; Wakita et al., 1998), and the Triassic Sadong and Kuching Formations of Sarawak (Breitfeld et al., 2017). For clarity, the present day coastline of Borneo is shown. However, (as noted in the text) the extensional basin setting of Sabah's ophiolite and sedimentary basins indicates protracted crustal extension through the Mesozoic and Cenozoic.

Journal Pre-proof

Data Tables

Table 1. Point counting data for the Segama Valley Felsic Intrusions. Mineral abundances presented here were calculated from point counted sections stained for plagioclase and K-feldspar. Point counting based on 300 points per sample. QAP modal mineral classifications are shown in Fig. 4.

Phase (%)	A245 Gd S.Purut	A249 Gd S.Danum	A261 Gd S. LKK	A265 Bt Gd S.LKK
Quartz	10.7	25.0	28.0	22.1
Plag	21.7	55.7	60.7	44.1
K-Fsp		5.0	3.0	3.3
Hornblende	16.0	0.7	3.3	17.1
Biotite		2.3		6.7
Magnetite	1.0	0.7	0.3	0.3
Chlorite	13.0	10.7	4.7	6.4
Sericite	37.7			
TOTAL	100.0	100.0	100.0	100.0
QAP %				
Quartz	33.0	29.2	30.5	31.7
Plag	67.0	65.0	66.2	63.5
K-Fsp	0.0	5.8	3.3	4.8
Classification	Tonalite	Tonalite	Tonalite	Biotite tonalite

Journal Pre-proof

Table 2. Zircon U-Pb data, sorted by sample then age. *Analysis identification, where x (recent Pb loss) and i (inherited grain) analyses were excluded from age calculations. †Percentage of common 206Pb estimated from the measured 204Pb. Common Pb correction not applied.

		U	Th	Pb		f206		±σ		±σ	$^{207}Pb/^{206}Pb$		$^{206}Pb/^{238}U$	
Sample	Spot*	(ppm)	(ppm)	(ppm)	Th/U	(%)†	$^{238}U/^{206}Pb$	(%)	$^{207}Pb/^{206}Pb$	(%)	age (Ma)	±σ	age (Ma)	±σ
A245	10	45	23	2	0.52	1.11	27.12	0.40	0.05	0.00	-	-	230.9	3.4
A245	5	40	21	2	0.54	0.85	26.71	0.44	0.05	0.00	81	400	235.0	3.9
A245	14	43	21	2	0.50	0.95	26.44	0.36	0.06	0.00	84	-	237.1	3.2
A245	9	77	44	3	0.58	0.50	26.43	0.34	0.05	0.00	115	226	238.2	3.1
A245	2	39	13	1	0.33	0.43	26.29	0.45	0.06	0.00	291	236	239.6	4.1
A245	1	54	26	2	0.49	0.47	26.27	0.53	0.05	0.00	140	-	239.7	4.8
A245	7	44	21	2	0.49	0.52	26.19	0.36	0.06	0.00	283	32	240.3	3.3
A245	11	83	38	3	0.47	0.26	26.09	0.35	0.05	0.00	221	-55	241.8	3.2
A245	8	76	47	3	0.64	0.32	26.00	0.36	0.05	0.00	230	112	242.5	3.3
A245	13	103	70	4	0.70	0.35	25.91	0.32	0.05	0.00	214	135	243.3	3.0
A245	4	92	58	4	0.64	0.04	25.99	0.38	0.05	0.00	346	59	243.3	3.5
A245	3	60	36	2	0.61	0.43	25.81	0.42	0.05	0.00	237	221	244.1	4.0
A245	12	53	24	2	0.46	0.42	25.59	0.44	0.05	0.00	-	-	246.1	4.2
A245	6	61	40	3	0.68	0.23	25.51	0.37	0.05	0.00	306	-	247.3	3.6
A249	1	56	31	2	0.58	0.78	26.06	0.41	0.06	0.00	246	-	240.9	3.8
A249	2	44	23	2	0.53	0.75	25.19	0.34	0.06	0.00	187	-	249.1	3.4
A249	3x	54	31	2	0.60	0.75	26.59	0.40	0.06	0.00	165	-	236.2	3.6
A249	5	40	20	2	0.52	0.30	25.04	0.30	0.05	0.00	265	-	251.7	3.0
A249	14	55	28	2	0.52	0.44	25.32	0.38	0.05	0.00	206	217	248.6	3.8
A249	12	95	53	4	0.57	0.26	25.18	0.31	0.05	0.00	250	116	250.5	3.1
A249	9	101	68	4	0.68	0.33	24.62	0.26	0.05	0.00	217	113	255.9	2.7
A249	11	59	31	2	0.54	0.84	25.75	0.42	0.05	0.00	16	194	243.6	4.0
A249	7	58	40	3	0.70	0.48	24.55	0.36	0.05	0.00	108	120	256.2	3.7
A249	4	61	47	3	0.79	0.29	25.23	0.32	0.05	0.00	164	-83	249.9	3.1
A249	13	51	27	2	0.55	0.54	24.92	0.37	0.05	0.00	63	-	252.3	3.7
A249	6	95	75	4	0.81	0.01	25.19	0.33	0.05	0.00	293	292	251.0	3.3
A249	8	45	24	2	0.54	0.33	25.28	0.41	0.05	0.00	128	-	249.3	4.1
A249	10	87	67	4	0.78	0.49	25.53	0.32	0.05	0.00	59	15	246.5	3.0
A261	11	80	34	2	0.44	0.39	36.99	0.54	0.05	0.00	170	-	171.3	2.5
A261	10	78	41	2	0.54	0.58	36.66	0.48	0.05	0.00	-	-	172.5	2.3
A261	8	165	109	5	0.68	0.28	36.60	0.45	0.05	0.00	53	113	173.3	2.1
A261	13	46	17	1	0.38	0.77	36.00	0.54	0.05	0.00	95	242	175.3	2.6
A261	12	193	199	6	1.06	0.01	35.82	0.41	0.05	0.00	301	-16	177.5	2.0
A261	9	109	116	4	1.09	0.46	35.60	0.55	0.05	0.00	112	196	177.8	2.7
A261	2	98	63	3	0.66	0.29	35.49	0.47	0.05	0.00	186	114	178.6	2.4
A261	5	174	122	5	0.72	0.13	35.33	0.44	0.05	0.00	260	137	179.7	2.3
A261	14	165	115	5	0.72	0.21	34.98	0.42	0.05	0.00	125	-57	181.3	2.2
A261	1	178	117	6	0.67	0.25	34.96	0.46	0.05	0.00	176	120	181.4	2.4
A261	3	81	47	2	0.59	0.16	34.84	0.45	0.05	0.00	199	-6	182.1	2.4
A261	6	195	192	7	1.01	0.27	34.80	0.39	0.05	0.00	15	20	182.2	2.0
A261	7	54	32	2	0.62	0.12	34.43	0.44	0.05	0.00	314	155	184.3	2.4
A261	4i	50	33	2	0.68	0.28	25.72	0.34	0.05	0.00	155	-	245.3	3.2
A265	3	234	156	7	0.68	0.56	36.70	0.45	0.05	0.00	30	224	172.3	2.1
A265	14	77	59	2	0.78	0.94	36.53	0.51	0.05	0.00	20	-	172.5	2.4
A265	2	139	105	4	0.78	0.42	35.87	0.45	0.05	0.00	82	-	176.5	2.2
A265	13	198	170	6	0.88	0.15	35.87	0.46	0.05	0.00	105	67	177.0	2.3
A265	1	128	89	4	0.71	0.45	35.77	0.50	0.05	0.00	167	-17	176.9	2.5
A265	12	80	64	3	0.83	0.02	35.43	0.57	0.05	0.00	231	-	179.4	2.9
A265	9	150	144	5	0.98	0.68	35.40	0.48	0.05	0.00	35	-	178.4	2.4
A265	10	312	325	11	1.07	0.37	35.34	0.42	0.05	0.00	99	84	179.2	2.1
A265	11	114	116	4	1.04	0.01	35.29	0.46	0.05	0.00	262	154	180.1	2.4
A265	7	140	104	4	0.76	0.39	35.15	0.43	0.05	0.00	1	-	180.1	2.2
A265	8	118	88	4	0.76	0.14	35.14	0.52	0.05	0.00	319	274	180.6	2.7
A265	6	173	118	5	0.70	0.19	35.10	0.46	0.05	0.00	218	-41	180.8	2.4
A265	5	478	340	15	0.73	0.06	35.05	0.42	0.05	0.00	149	-58	181.2	2.2
A265	4	321	194	10	0.62	0.33	35.03	0.42	0.05	0.00	63	28	180.9	2.1

Journal Pre-proof

Table 3. Whole rock major and trace element data. *Sample preparation method: F, sample fused prior to acid dissolution; HF, sample dissolved without prior flux fusion.

Lat.			4.947333	5.014017	5.094228	5.084223	4.948658
Long.			117.74274	117.725785	118.013355	118.019607	117.746
Height (AMSL), m			1183	737	291	178	1328
			Gd S. Purut	Gd S. Danum	Gd S. LKK.	Bt Gd S. LKK.	Basalt S. Purut
Element	Prep.*	Analysis	A245	A249	A261	A265	A247
(wt%)							
SiO_2	F	XRF	56.20	61.57	67.95	55.59	46.28
TiO_2	F	XRF	0.83	0.51	0.18	0.63	0.73
Al_2O_3	F	XRF	16.95	15.21	15.86	17.55	16.39
FeO_{TOT}	F	XRF	7.03	4.32	1.50	6.40	7.11
MnO	F	XRF	0.15	0.08	0.05	0.14	0.21
MgO	F	XRF	3.95	1.86	0.53	3.35	2.07
CaO	F	XRF	6.66	4.13	3.15	6.96	12.82
Na_2O	F	XRF	3.50	4.91	6.28	3.41	2.72
K_2O	F	XRF	1.49	1.96	1.96	2.11	0.59
P_2O_5	F	XRF	0.17	0.12	0.06	0.17	0.14
Total			99.84	99.47	99.80	99.25	99.63
LOI			2.13	4.33	2.12	2.22	9.76
ppm							
Ta	F	ICP-MS	0.22	0.27	0.08	0.24	0.09
Sc	HF	ICP-MS	22.59	10.99	1.47	18.54	24.53
V	HF	ICP-MS	180.80	87.87	26.95	241.50	225.60
Cr	HF	ICP-MS	89.33	26.75	0.68	8.09	35.02
Ga	HF	ICP-MS	15.56	14.06	14.53	18.61	14.98
Co	HF	ICP-MS	22.46	11.81	2.34	20.39	18.56
Ni	HF	ICP-MS	36.98	13.28	1.03	9.09	17.07
Cu	HF	ICP-MS	35.57	10.63	20.49	84.94	18.44
Zn	HF	ICP-MS	54.62	43.77	35.45	61.22	97.94
Cs	F	ICP-MS	0.28	2.08	-0.05	1.86	0.23
Rb	HF	ICP-MS	33.04	55.68	13.16	31.66	12.23
Ba	HF	ICP-MS	181.10	204.40	363.50	416.40	56.24
Sr	HF	ICP-MS	345.40	220.90	673.30	567.30	320.80
Zr	F	ICP-MS	159.90	223.20	112.50	75.65	43.59
Hf	F	ICP-MS	4.03	5.53	2.72	2.11	1.17
Th	F	ICP-MS	3.40	4.19	0.73	3.88	0.34
U	F	ICP-MS	1.22	1.19	0.28	0.95	0.14
Pb	HF	ICP-MS	2.75	3.32	5.41	6.86	1.13
Nb	F	ICP-MS	3.21	3.48	1.57	4.11	1.45
Y	F	ICP-MS	30.13	28.67	4.72	19.31	16.27
La	HF	ICP-MS	9.48	13.41	5.36	11.90	3.41
Ce	F	ICP-MS	25.04	32.16	11.89	28.24	8.12
Pr	F	ICP-MS	3.82	4.45	1.56	3.98	1.34
Nd	F	ICP-MS	15.79	16.83	4.68	14.68	6.84
Sm	F	ICP-MS	4.66	4.39	1.23	3.77	1.92
Eu	F	ICP-MS	1.30	1.06	0.50	1.11	0.65
Gd	F	ICP-MS	5.03	4.37	1.03	3.58	2.36
Tb	F	ICP-MS	0.80	0.71	0.13	0.51	0.40
Dy	F	ICP-MS	4.77	4.31	0.81	2.99	2.50
Ho	F	ICP-MS	0.99	0.91	0.17	0.63	0.53
Er	F	ICP-MS	2.72	2.58	0.37	1.67	1.49
Tm	F	ICP-MS	0.26	0.25	-0.07	0.11	0.22
Yb	F	ICP-MS	2.88	2.88	0.56	1.84	1.46
Lu	F	ICP-MS	0.46	0.47	0.11	0.29	0.24

Journal Pre-proof

Table 4. Whole rock radiogenic isotope data.

	Sample	$^{87}Sr/^{86}Sr$	2SE	$^{143}ND/^{144}Nd$	2SE	$^{206}Pb/^{204}Pb$	2SE	$^{207}Pb/^{204}Pb$	2SE	$^{208}Pb/^{204}Pb$	2SE
S. Purut tonalite	A245	0.703845	09	0.51299	07	19.3276	23	15.5857	24	38.9625	75
S. Danum tonalite	A249	0.705354	10	0.51296	13	18.9355	26	15.5659	24	38.7117	69
S. LKK. tonalite	A261	0.703227	11	0.513097	13	18.6973	12	15.5621	11	38.3783	41
S. LKK. Bt tonalite	A265	0.703486	12	0.51292	08	18.7302	14	15.5837	12	38.6578	45
S. Purut basalt	A247	0.703768	13	0.513036	15	19.0022	25	15.5537	02	38.4495	54

Journal Pre-proof

Table 5. Zircon oxygen and Hf isotopic data. Oxygen values are mean and 1 SD error (sum of internal and external precision) for all analysed samples (excluding the grains identified for Pb loss or inheritance in Table 2).

	Sample	SiO2	$\delta^{18}O$ Zrc	Err.	$^{176}Hf/^{177}Hf$	SD
S. Purut tonalite	A245	56.2	4.83	0.39	0.283036	15
S. Danum tonalite	A249	61.6	4.74	0.26	0.283027	08
S. LKK. tonalite	A261	68.0	5.04	0.28	0.283045	20
S. LKK. Bt tonalite	A265	55.6	5.02	0.24	0.283028	18

Journal Pre-proof

CRediT author statement

Burton-Johnson, A. – Conceptualization, Methodology, Software, Validation, Formal analysis, Investigation, Data Curation, Writing - Original Draft, Writing - Review & Editing, Visualization, Project administration, Funding acquisition

Macpherson, C.G. – Resources, Writing - Original Draft, Supervision, Project administration, Funding acquisition

Millar, I.L. – Investigation, Resources, Writing - Original Draft (analytical methodology)

Whitehouse, M.J. – Investigation, Resources, Writing - Original Draft (analytical methodology)

Ottley, C.J. – Investigation, Resources

Nowell, G.M. – Investigation, Resources

Journal Pre-proof

Declaration of interests

☒ The authors declare that they have no known competing financial interests or personal relationships that could have appeared to influence the work reported in this paper.

☒The authors declare the following financial interests/personal relationships which may be considered as potential competing interests:

N/A

Journal Pre-proof

Graphical abstract

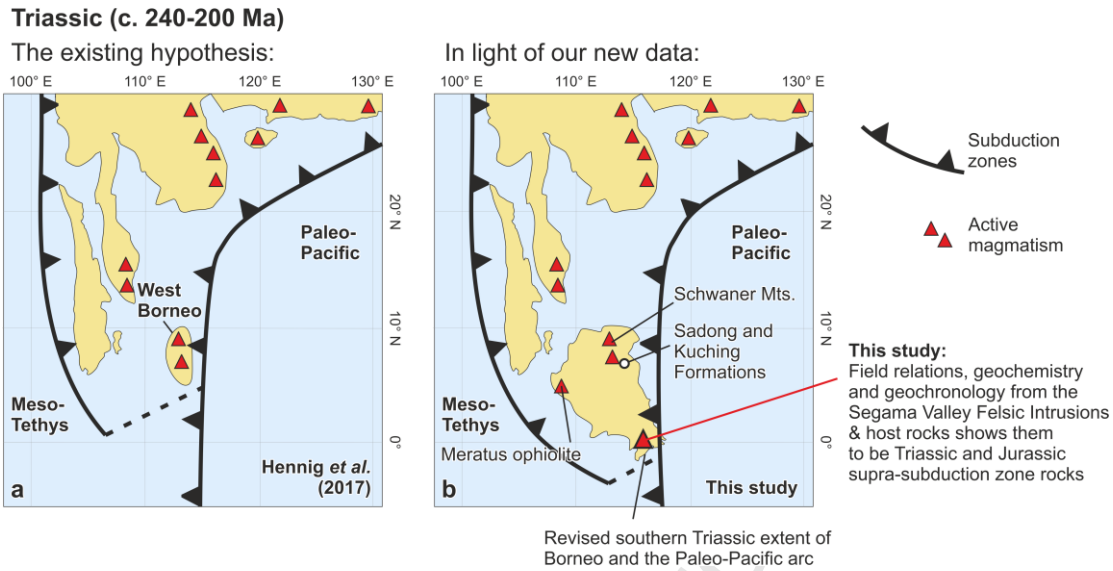

Journal Pre-proof